Staining and extraction protocol for lipid droplets in *Malassezia globosa* and analysis of consumed and secreted lipids during the growth phase

Catherine Eliana Cabrera Díaz

A thesis presented in partial fulfillment of the requirement for the degree of Master in Chemistry

Supervisor:

Elizabeth Jiménez Díaz Ph. D.

Co-supervisor:

Adriana Marcela Celis Ramírez M.Sc, Ph.D.

Grupo de investigación en bioquímica aplicada (GIBA)

Grupo de investigación celular y molecular de microorganismos patógenos (CeMoP)

Universidad de los Andes

Faculty of Science – Department of Chemistry

Bogotá, Colombia

June 2020

Acknowledgments

First of all, I want to thank Professors Elizabeth Jiménez and Adriana Celis for their instruction and collaboration throughout this work.

I also want to thank all my family and Andrés Pérez for their unconditional support during each facet of this work.

I'm also grateful with my co-worker María Juliana Mantilla, who was fundamental during each stage of this journey.

On the other hand, I want to thank my other co-workers from both research groups, GIBA and CeMoP, for helping me whenever I needed it.

Also, I want to acknowledge μ-core in Universidad de los Andes especially Humberto Ibarra, Juan Orozco for supporting me with the use of the confocal microscope.

On the other hand, I want to point out the help I get from MetCore in Universidad de los Andes with the run and subsequent analysis of lipidomic data. Especially I want to thank Mónica Cala, María José Santander and Adriana Romero for helping me in this stage of the project.

I would also like to thank the department of biological sciences, especially Harold, Luz Marina, Angelica and the entire sterilization team at the Universidad de los Andes, for giving me the space and materials to carry out this work when needed.

Lastly, I would like to thank the chemistry department, who will help me during my education in these two years and provide me with the space and resources to work.

Agradecimientos

En primer lugar, quiero agradecer a las profesoras Elizabeth Jiménez y Adriana Celis por sus enseñanzas y colaboración a lo largo de este trabajo.

También quiero agradecer a toda mi familia y a Andrés Pérez por su a apoyo incondicional durante cada faceta del desarrollo de este trabajo.

Adicionalmente quiero agradecer a mi compañera de trabajo María Juliana Mantilla, la cual me acompaño durante cada etapa de esta travesía, complementando mis ideas y ayudando con el correcto desarrollo de este proyecto.

Por otra parte, deseo agradecer a mis compañeros de trabajo de ambos grupos de investigación, GIBA y CeMoP, los cuales me ayudaron en cada momento que lo necesité.

Asimismo, quiero brindar un agradecimiento a μ-core especialmente a Humberto Ibarra, Juan Orozco por apoyarme con el uso del microscopio confocal.

Por otra parte, quiero agradecer a met-core, en especial a Mónica Cala, María José Santander y Adriana Romero por ayudarme con la corrida y posterior análisis de datos de lipidómica.

También me gustaría dar un agradecimiento al departamento ciencias biológicas, especialmente a Harold, Luz Marina, Angélica y todo el equipo de esterilización de la Universidad de los Andes, que me brindaron el espacio y los materiales para desarrollar este trabajo.

Por último, me gustaría dar un agradecimiento al departamento de química, los cuales me ayudaron durante mi educación en estos dos años de maestría y me brindaron el espacio y recursos para trabajar.

Content table

Abbreviations table

AhR	Arylhydrocarbon receptor
APCI	Atmospheric-pressure chemical ionization
CAR	Acylcarnitine
CE	Cholesteryl ester
Cer	Ceramides
CL	Cardiolipins
CW	Calcofluor white
ESI	Electrospray ionization
ER	Endoplasmic reticulum
FAHFAs	Fatty acid esters of hydroxy fatty acids
FAS	Fatty acid synthase
FA	Fatty acids
GlcCer	Glucosylceramides
GPLs	Glycerophospholipids
HPLC	High performance liquid chromatography
LD	Lipid droplets
LP	Lysophospholipids
MALDI	Matrix-assisted laser desorption/ionization
MS	Mass spectrometry
NR	Nile Red
QTOF	Quadrupole time-of-flight
PCA	Principal component analysis
PC	Phosphatidylcholine
PE	Phosphatidylethanolamine
PFA	Paraformaldehyde
PV	Pityriasis versicolor
SM	Sphingomyelin
SL	Sphingolipids
SE	Sterol esters

ST	Sterol lipids
TAG	Triacylglycerols
UHPLC	Ultra-high performance liquid chromatography

Figures list

Tables list

I. Abstract

Malassezia yeasts are lipophilic and lipid-dependent. It is found in the microbiota of humans and animals skin. This genus has been associated with different skin disorders, and fungemia in humans, mainly in neonates and immunocompromised patients, especially those who receive lipid supplements. Several reports estimate that dandruff and seborrheic dermatitis, diseases related to *Malassezia*, are some of the most common skin conditions, affecting half of the world population. Despite its high prevalence, much remains to be discovered about the pathophysiological processes triggering its pathogenicity.

Within the lipid metabolism of *Malassezia*, the presence of lipid droplets (LDs) has recently been reported. These are organelles present in multiple organisms, including mammals, algae, yeast, and others. Considering *Malassezia* dependency on lipids, particular interest has been directed to the study of these organelles. In this project, the standardization of a double staining protocol to identify LDs, the implementation of a LD extraction protocol, the dynamics of LDs formation in *M. globosa,* and consumed and secreted lipids analysis of the yeast were performed. To achieve these goals, three different fluorophores for LD staining were used: Nile Red, BODIPY 493/503, and LipidTOX deep red neutral using Calcofluor White for cell wall staining. Afterward, LD dynamic formation was explored. It was found that LDs starts forming in *M. globosa* after 24 hours post-cultured during the exponential phase growth. LDs size range increased in the stationary phase from ~0.5 μm^2 to ~1.5 μm^2, and up to ranges ~1 μm^2 to 6 μm^2. Also, LDs numbers per cell decrease when entering to stationary phase. Thus, the proportion between LDs vs. cell area varied more when reaching to late stationary phase. Based on these observations, it is proposed that LDs coalescence while yeast enters to different growth phases. In other hand, LDs extraction protocol was adequately implemented in *M. globosa*, however, further purification procedures are needed in order to remove cellular residues from LDs solution.

Besides, as lipids are relevant in the pathophysiology of diseases, getting a better comprehension of *Malassezia* secretome and its possible interaction with the skin would allow to have a better insight in this regard. This project aimed to study the consumption and secreted lipids by *Malassezia globosa* using lipidomic approaches. To achieve this, fresh mDixon as control and mDixon supernatant of the yeast cultured up to 72 h and 90 h were studied. Lipid extraction was performed by a modified Bligh and Dyer method followed by solid-phase extraction. Lipidomic analysis was conducted by HPLC-ESI-QTOF in positive ionization mode. Lipid profiles from mDixon, early, and late

stationary phases were differentiated via principal component analysis (PCA). The analysis mainly showed the presence of different phospholipids, cardolipines, bile acids and ceramides. In general, there was a higher percentage of lipids consumed by *M. globosa* in comparison to the secreted lipids. Further analysis is needed to confirm the identity of each individual lipid.

II. Introduction

Malassezia is a genus of lipophilic and lipid-dependent yeast found in the microbiota of humans and animals skin.[1,2] *Malassezia* secrete enzymes such as lipases and phospholipases, to exploits the essential nutrients for their growth without causing disease. The yeast obtain these sources of nutrients from sebum, a lipid-rich substance, produced by the sebaceous glands.[3,4] However, perturbation of this process might be connected in the establishment of some skin diseases.[5,6] This genus has been associated with different skin disorders and fungemia in humans, mainly in neonates and immunocompromised patients, especially those who receive lipid supplements.[1,3,4,7,8] Up to now, 18 species of *Malassezia* has been described and included in three principal clades. Clade B is related to the most common human skin resident species, such as *M. restricta* and *M. globosa*.[9,10] These species are clinically relevant because they are highly related to different diseases such as dandruff/seborrheic dermatitis and pityriasis versicolor (PV), both common skin infections.[11] Taking into account this information, this project focuses on *M. globosa*.

Lipid dependent characteristic is due to the absence of fatty acid synthase (FAS). This is a multifunctional enzyme necessary for *de novo* synthesis of palmitic acid, a fatty acid (FA) that serve as a source for the synthesis of long-chain FA.[2] In counterpart, *Malassezia* has a high number of genes encoding secreted enzymes hydrolases such as lipases, phospholipases, sphingomyelinases, responsible of degrading sebum.[2,5,7,12] After *Malassezia* obtains the lipids from the skin environment, these molecules can enter to the yeast and have various chemical processes such as elongation, β-oxidation or storage.[4]

Within the lipid metabolism of *Malassezia*, the presence of LDs has recently been reported.[12] In other species, these organelles have a function associated with the regulation of FAs availability in cells, participating in the membrane formation and maintenance, energy homeostasis, energy storage, lipid metabolism, and signal transduction in cells.[13,14] It is speculated that LDs may play an important role in *Malassezia* due to its lipid-dependent nature and this is the interest in the study of these organelles in this yeast. In this project, the dynamics of LDs formation in *M. globosa* and extraction protocol of this organelle for future analysis will be explored.

Also, lipids are required in multiple cellular processes such as cell signaling, energy supply and membrane formation among others.[15] In *Saccharomyces cerevisiae*, FA act as basic building blocks for the synthesis of membrane lipids such as glycerophospholipids (GPLs), sphingolipids (SL) and storage lipids such as triacylglycerols (TAGs) and sterol esters (SE). GLPs, SLs and sterols (ST) are essential membrane components, maintaining its integrity and allowing the viability of yeast cells. In other hand, storage lipids serve as energy source and precursors for membrane synthesis.[15,16] As well, lipids has been related with the regulation in pathogenic traits in some yeast.[17] Recently a mass spectrometry based lipidome and a gene prediction analysis lipid metabolic proteins was described for six different *Malassezia* species.[18] Such investigation provide a general overview of the lipid composition and metabolism of these yeast. Nevertheless, a number of questions regarding the role of lipids *Malassezia* life cycle remain open. In order to delve into the preference of lipid consumption and secretion in different growth stages, this project also aims to study *M. globosa* consumed and secreted lipids using lipidomic approaches.

III. Theoretical framework

The skin is the largest organ in the human body composed of two anatomic units, dermis, and epidermis. The last one is a simple stratified epithelium consisting of four principal layers, from the basal to the most superficial: the basale, spinosum, granulosum, and corneum stratum. In cellular terms, it is principally composed of keratinocytes, melanocytes, langerhans cells, merkel cells and other inflammatory cells (**Figure 1**).[19,20] Keratinocytes born in the basale stratum and proliferate toward the corneum stratum until they commit to differentiate and migrate towards the surface of the epidermis.[20]

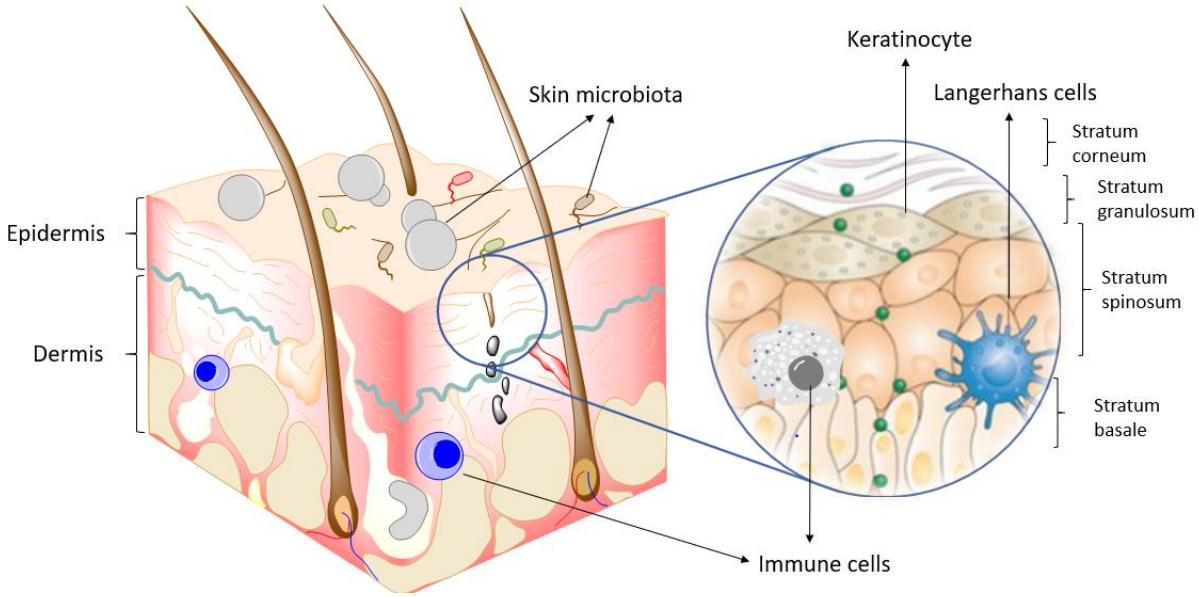

Figure 1. Human skin conformation. Based on Kaplan. D and collaborators, 2012.[20]

Functions of the skin include the prevention from water loss, toxin excretion, protecting barrier due to mechanical resistance and immune response.[19] This organ is part of the innate immune system of the human body, acting as the first line of defense of the body against microorganisms. This occurs through the skin water content, acidic pH, presence of antimicrobial lipids, and local microbiota.[19,21] Also, it is known that skin microenvironment promotes the establishment and coexistence of a diversity of commensal microorganisms.[22] Specifically for yeast, culture-based studies have reported *Malassezia, Rhodotorula, Debaromyces,* and in some sites, *Candida* as fungal skin commensals.[23] Between them, *Malassezia* has shown predominance in multiple body sites such as, back, external auditory canal, glabella, hypothenar palm, inguinal crease, manubrium, nare, occiput, retro auricular crease , and volar forearm. One of the main species is *M. globosa* followed

by *M. restricta* and *M. sympodialis*.[22,24] However, they can also act as commensals and pathogens in the skin.[25]

Malassezia is a genus belonging to the phylum Basidiomycota. It is a lipophilic and lipid-dependent yeast part of the microbiota of humans and animals skin.[1,2] This yeast was first isolated around the XIX century in patients with PV, initially classified as *Microsporon furfur*.[26] From that moment and assisted by molecular techniques, it´s taxonomical classification has been matter of multiple revisions in the last decades.[8,10,25] *Malassezia* have been reported from several sources, such as nematodes, sponges, corals, different mammals, and even in environmental samples.[10,25] Nowadays, 18 species of *Malassezia* has been discovered and classified in the main clusters or clades. According to Wu and collaborators; cluster A consists of fungemia-causing species *M*. *furfur* and three other species: *M*. *japonica*, *M*. *obtusa*, and *M*. *yamatoensis*, rarely found on healthy human skin; cluster B includes the most common human skin residents, which are *M*. *globosa* and *M*. *restricta* and slightly less common in human skin *M*. *sympodialis* among others. Cluster C consists of two outliers, *M*. *cuniculi*, and *M*. *slooffiae*, which are rare on human skin.[9]

This yeast has been associated with a variety of skin conditions such as dandruff, atopic eczema, seborrheic dermatitis, PV, and folliculitis.[25,27] Some reports estimate that dandruff and seborrheic dermatitis can affect half of the world population. The group of the newborn child's is one of the most prominent incidence groups (up to 42%).[27] Additionally, in immunocompromised patients, including AIDS/VIH patients, organ transplant patients, and lymphoma patients, *Malassezia* can cause systemic infections.[28] Also, it has been described that *Malassezia pachydermatis* besides cause otitis and dermatitis in canines, can generate invasive infections in neonates, especially those who receive lipid supplements.[3,4,6,8,28]

Considering the wide range of diseases that *Malassezia* can cause, it could be described as a multifaceted organism, which change its phenotype according to patient health status. Velegraki and collaborators enunciated in 2015 the different facets of this yeast.[6] As commensal and pathogenic phenotype state could be modified based on the interaction of the microorganism with the immune system in the following ways:[6]

1. In healthy skin, *Malassezia* acts as a commensal organism.
2. Alterations in melanocyte function can induce the appearance of hypopigmented or hyperpigmented macules. These can generate an absence of inflammation and mild change in epidermal function, developing a PV phenotype.

3. When *Malassezia* causes inflammation patterns without developing immunity mediated with antibodies, it can generate dandruff and seborrheic dermatitis phenotype.
4. Induction of specific immune response can develop atopic dermatitis phenotype.
5. Some species of *Malassezia* can cause folliculitis, an invasion and inflammation in hair follicles.

The absence of de novo synthesis of FAs in *Malassezia* is related with the requirement to exploit lipid sources from its medium. For this purpose, *Malassezia* secrete lipases, phospholipases, lipoxygenases and sphingomyelinases in order to supply its lipid requirements.[2,5,7,12] Uptake of these resources are necessary for their subsequent use in lipid-biosynthesis routes, required to sustain the growth of *Malassezia* species.[2] In healthy patients, the consumption of lipids from the sebum is carried out efficiently, so no damage is inflicted on the patient.

Malassezia genus shows different lipid-assimilation phenotypes, having versatile lipid-dependent species as *M. pachydermatis* to more restricted species like *M. globosa* and *M. restricta.*[2,7,9] These metabolic variances among species can be related with the differences in the pathogenic role of these species and in the development of certain dermatological diseases.[2,7,29] The production of lipases and phospholipases is consider a pathogenic factor in the skin disease associates with *Malassezia.*[30] Among several *Malassezia* species, *M. globosa* have shown the highest lipase activity, which can provide an explanation as why this specie is an important pathogenic specie in several human skin disease (**Figure 2B**).[30,31] Additional, pathogenic phenotype can be affected by the expression of various bioactive indoles that act in the skin through the arylhydrocarbon receptor (AhR), which is expressed on almost all cell types found in the epidermis (**Figure 2A - 2C**).[5,6,32] The indoles molecules can also modify the expression of cytokines, chemokines and antimicrobial peptides of the skin, interfering with UV damage of the skin (**Figure 2C**).[32]

As stated before, the pathogenicity of this yeast is related to the production of proteases, lipases, phospholipases, lipoxygenases, among others.[33,34] The expression of these enzymes could be under the action of proper agonist or antagonist like endorphin-β (**Figure 2B**).[35] Besides, zymogens or AhR ligands are capable of activating the complement immune system, causing damage in keratinocytes. These events cause the appearance of *Malassezia* associated symptoms such as epidermal spongiosis, inflammation, and itching (**Figure 2C**).[6]

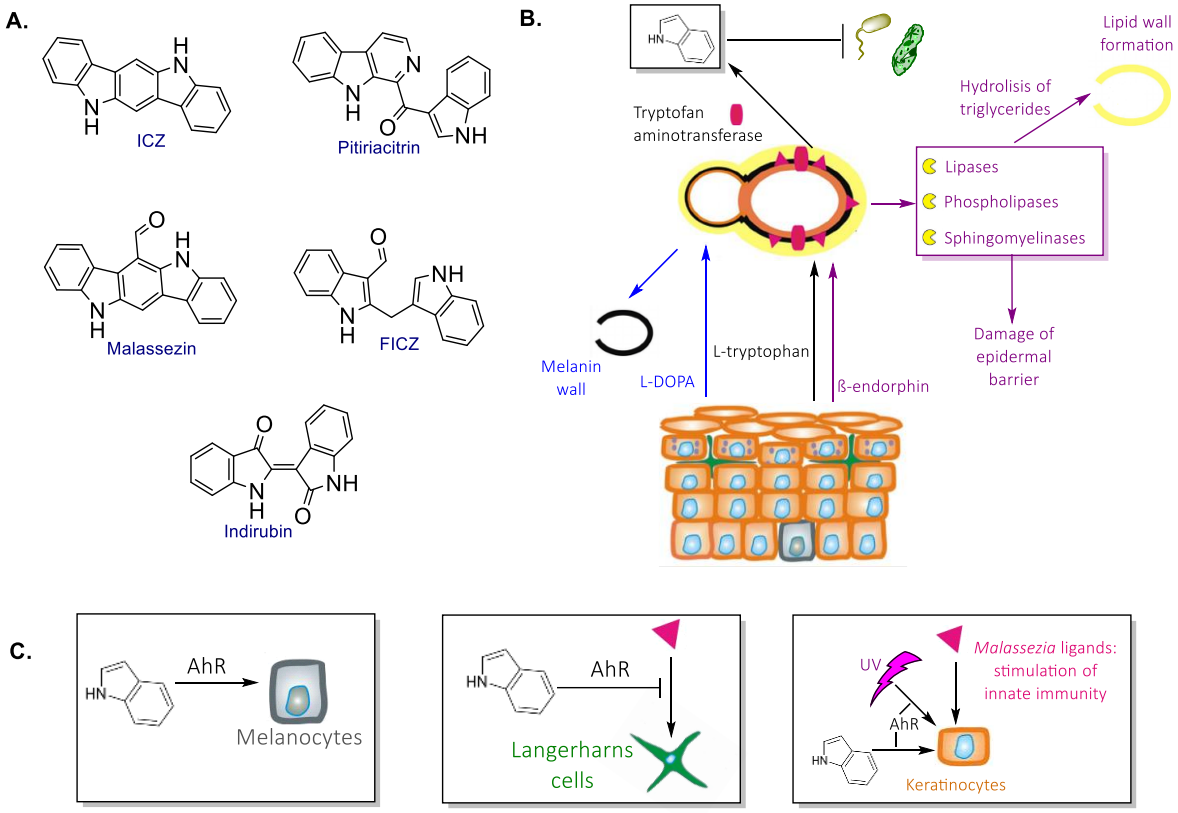

Figure 2. *Malassezia* interaction with the skin. **A**. Structure of bioactive indoles that act in the skin through the arylhydrocarbon receptor (AhR) **B.** Different interactions of *Malassezia* and the epidermis of the skin. In blue, the synthesis of the melanin cell wall. In black, the synthesis of bioactive indoles. In purple the activity of different hydrolases. **C.** Interaction between the indole molecules and other *Malassezia* ligands with different skin cells. Based on Velegraki and collaborators, 2015.[6]

Now, lipids are a group of compounds with crucial biological functions, including energy storage, signaling processes and as structural components of the cell membranes.[36,37] Unlike the case of genes and proteins, lipid structures are generally more diverse and complex, contributing to the development of multiple classification systems.[38,39] In 2005, a modern, robust classification lipid system defines these molecules as "hydrophobic or amphipathic small molecules that originate entirely or in part by carbanion-based condensations of thioesters and/or by carbocation-based condensations of isoprene units".[36,38] Based on this classification; eight lipid categories were defined: glycerolipids, SL, GPLs, ST, FA, prenol lipids, polyketides, and saccharolipids (**Figure 3**).[36,37,40] This classification cover lipids originated in eukaryotes, prokaryotes and archaea.[39]

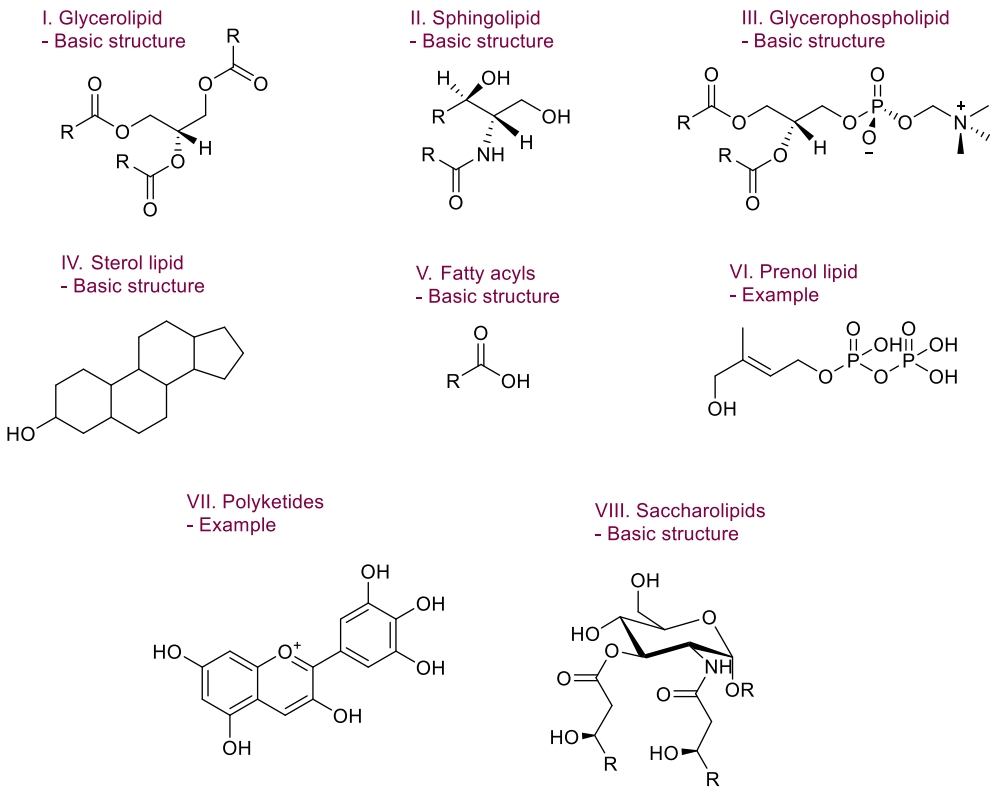

Figure 3. Lipid families according to the International Lipids Classification and Nomenclature Committee, with one representative structure for each family.

Lipid versatility among different organisms convert lipid biology on a significant research target. To describe the major lipid profile within a cell, tissue, or organism, different lipidomics approaches have emerged in the last years.[37,40] This is a relatively new field of research in which different analytical techniques such as nuclear magnetic resonance, Raman spectroscopy, mass spectrometry (MS) even computational methods allowing to get an insight into the lipidome of multiple biological systems.[36,38] Among the different approximations, MS-based techniques have been widely used due to their availability and accurate identification of lipids, its high sensitivity allowing the identification of molecules up to picomolar concentrations, quantification, and monitoring of lipid profiles in complex biological mixtures.[36]

Lipidomics MS approximation can be performed by two approximations, shotgun lipidomics, which involve the direct injection of the extracted sample into a mass spectrometer or chromatography-based lipidomics, where a separation of the sample prior the injection to the mass spectrometer is done.[41] The first approximation allows to control changes in specific lipid species quickly. By the other hand chromatography separation, usually is done via high proficiency liquid chromatography (HPLC) or ultra-high performance liquid chromatography (UHPLC), allowing to have a different

resolution among components in a sample.[37] Different ionization methods including electrospray ionization (ESI), Matrix-assisted laser desorption/ionization (MALDI) and atmospheric-pressure chemical ionization (APCI) can be used. Nowadays, these are the ionization techniques of choice for complex lipids with molecular mass higher than 500 Daltons. Also, different mass spectrometers like a quadrupole time-of-flight (QToF) are used for lipid characterization. This instrumentation provides a resolution of up to 40,000 and high mass accuracy. Additional TOF analyzers have extremely high scan rate and high ion transmission. However, it usually has a limited dynamic range of the detector, allowing quantification only in a narrow concentration range.[42]

IV. State of the art

The presence of LDs has recently been reported in *Malassezia*, possibly related to the lipid metabolism.[12] LDs are intracellular organelles found in the majority of cells. They have a highly dynamic role in metabolism, especially when exposed to high FA diets.[43,44] Their basic structure consists of a hydrophobic neutral lipid core compose predominately but not exclusively of TAGs and SE. TAGs are the product of diacylglycerol acyltransferases (DGTA1, DGTA2, DGA1, and Lro1); meanwhile, SE is made by acyl-CoA:cholesterol O-acyltransferases (ACAT1 and ACAT2; Are1p and Are2p).[13] Other lipids within the core are retinyl, waxes, lipid esters, and squalenes. The outer core of LDs is composed of a phospholipid monolayer with multiple host proteins such as perilipins and seipins (**Figure 4**).[45,46] GLPs are fundamental for LD stability based on their amphiphilic characteristics, which allow them to work as surfactants.[44,47] The size of these structures can vary among different organisms.

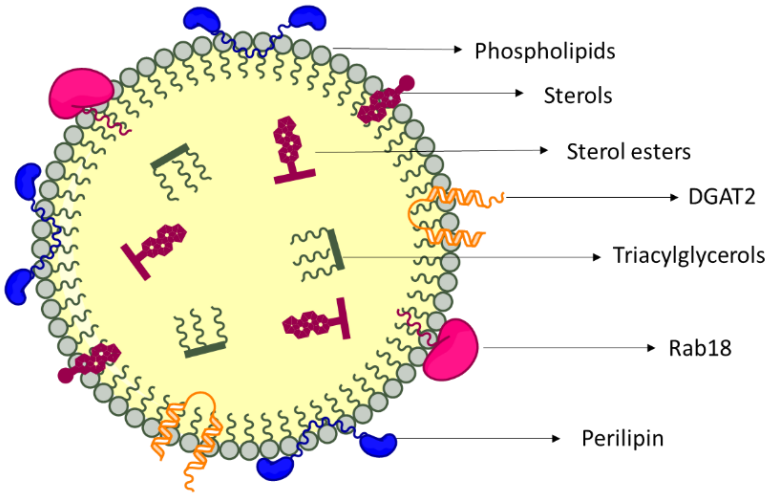

Figure 4. Lipid droplet morphology. Based on Martin. M, 2011.[46]

The formation of LDs is a complex process that relies on several factors. It is known that these structures are formed between the clefts of the endoplasmic reticulum (ER).[44,48] During the transition between the bilayer of ER and the formation of an LD monolayer, a structural change in the ratio of specific lipids has been reported. In that process, the concentration of PC increases while the level of cholesterol and sphingomyelin decreases.[44,49] To achieve this compositional change, metabolic intermediates such as DAGs or FA accumulate on the LD surface. This process increases the diffusion rate of phospholipids, acting as co-surfactants, decreasing the superficial tension of the micelle and allowing the LD formation.[44]

Recent studies have shown that during the maturation period of LDs, these structures are retained in the ER by a thin membrane or embedded in this organelle. Whether this organelle is released by the ER or not depend on the composition of the lipid intermediates in the biogenesis sector of LDs. Some proteins such as the fat storage-inducing transmembrane protein 2 (FIT2) or Ras-related protein RAB18 also have a fundamental role in this maturation process by increasing the accumulation of DAG and promoting the disengage of LD from the ER.[13,47,50]

Based on this information, three models for lipid droplet formation have been proposed (**Figure 5**). The first one and most accepted in this field establishes that the lipidic neutral core exscinds through a budding process from the external layer of the ER. This process is mediated by lipid droplet proteins (PAT proteins like perilipins), which allows forming LDs in specific sites of ER. The second model establishes that LD exscind from both layers of ER, creating a vesicle. The last theory proposes that LDs are shaped through the formation of a bicelle by hatching, and afterward, the establishment of the monolayer membrane through the micelle-like isolation of the inner membrane leaflet in the LD lumen.[47,48]

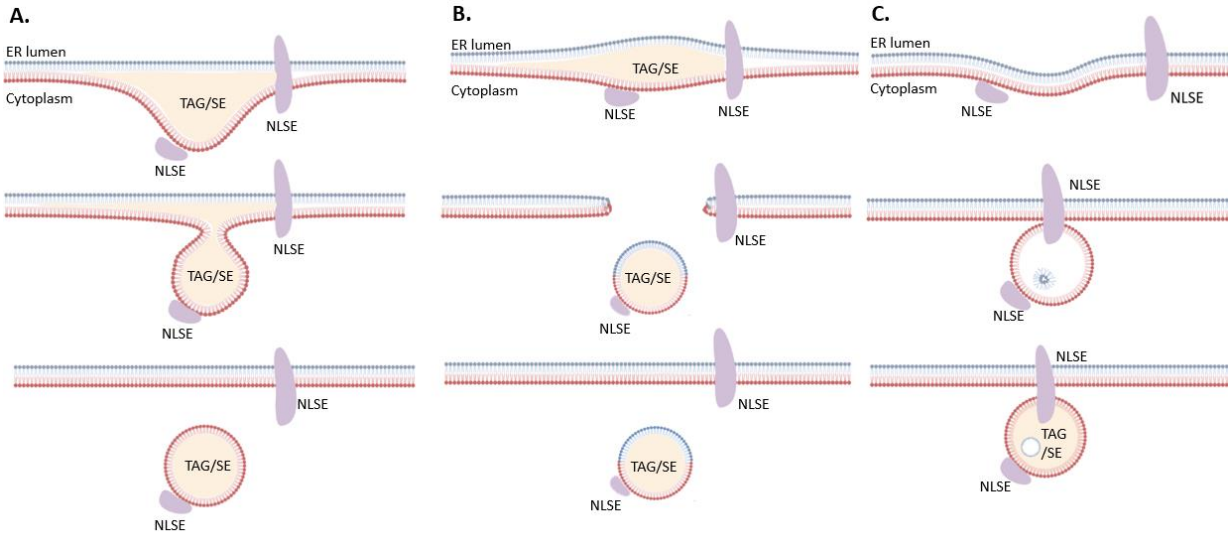

Figure 5. Formation of the LD in the endoplasmic reticulum. Left: First model, budding LD model from RE. Center: Second model, excision of the LDs. Right: Third model, Bicelle formation. NLSE: Neutral Lipid Synthesis Enzymes Taken from Onal and collaborators, 2017.[48]

In general, yeast metabolism fulfills its cellular lipid requirements by different pathways including the uptake of external lipids and *de novo* synthesis of lipids.[15] However, an excess of cellular lipids can be harmful to the cell and may lead to lipotoxicity. To overcome this effect, lipids are storage in

LDs.[12,15,49] Based on this idea, LD formation depends on the balance between lipid arrival and consumption of the cell.[51] To store lipids inside LD, it is necessary to esterify and convert them into TAGs and SEs to exclude water.[43,44,49] It´s known that in proper growth conditions, such as fresh medium, lipids rapidly utilize by yeast when they are presented for rapid membrane synthesis and as metabolic precursors, however, when cells sense stress or lack of required nutrients, the accumulation of neutral lipids is trigger within the cell.[52] This process can occur through different metabolic pathways like the glycerol-3-phosphate and monoacylglycerol pathway for the formation of TAGs and the sterol ester synthesis pathway for SEs (**Figure 6**). Considering this, comprehending the variations in lipid consumption through time will give important insight within the formation and dynamics of LDs.

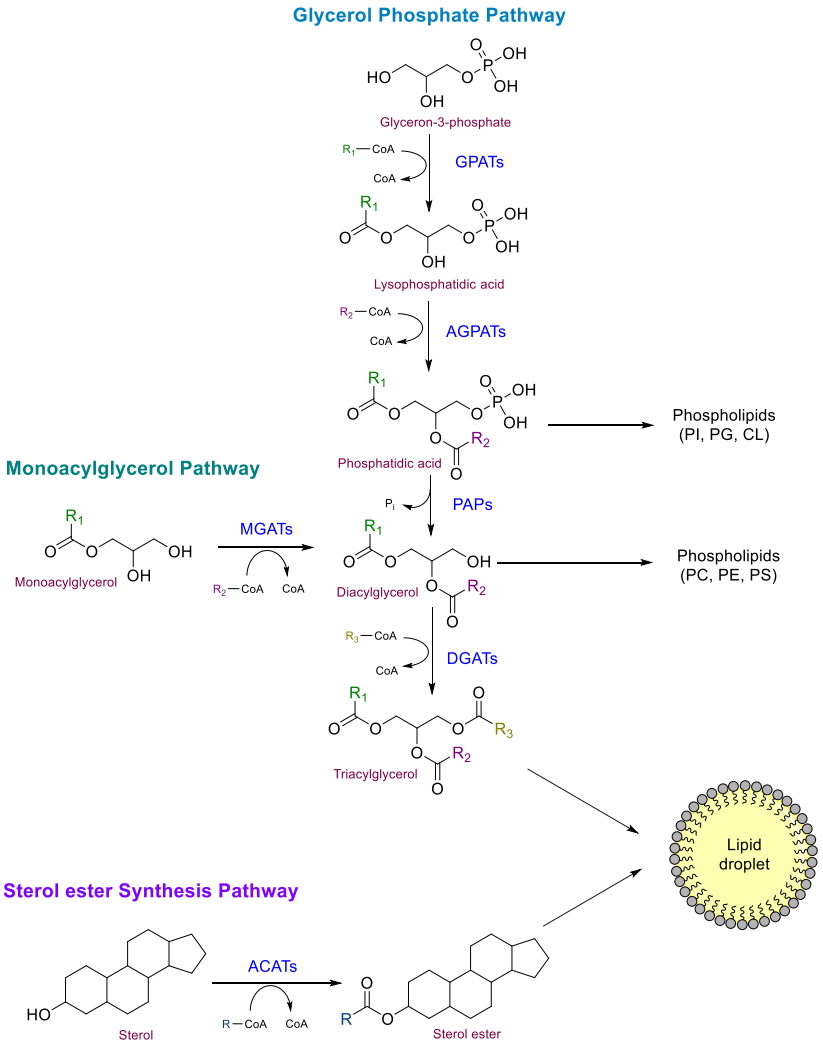

Figure 6. Metabolic pathway of triglycerides and sterol ester synthesis. De novo triglycerides synthesis through the glycerol-3-phoshate pathway involve four steps mediated by the following enzymes: glycerol-3-phosphate O-

acyltransferase (GPATs), 1-acylglycerol-3-phosphate O-acyltransferase (AGPATs), phosphatidic acid phosphatase (PAPs) and diacylglycerol acyltransferase (DGATs) enzymes. Also, triglycerides synthesis can occur through the monoacylglycerol pathway mediated by the monoacylglycerol acyltransferase (MGATs) enzymes. The synthesis of sterol esters is conducted by acyl-CoA cholesterol O-acyltransferases (ACATs). Based on Onal and collaborators, 2017.[48]

Routes related to the synthesis of neutral lipids has been described in *Malassezia.*[18] In order to fulfill its lipid metabolic requirements, *Malassezia* obtains the lipids from the skin environment and use this molecules in various chemical processes such as elongation, β-oxidation or storage.[4] Specifically, consumed FAs can be activated by the acyl-CoA synthases FAA1/2/3/4, present in different *Malassezia* strains.[18] From here, FAs can be converted to phosphatidic acid (PA) and latter one to GLPs through the CDP-DAG metabolic route or via the Kennedy pathway.[18,53,54] In *Malassezia* case, genes associated with the CDP-DAG metabolic route has been found in *M. globosa*, *M. restricta*, *M. furfur*, *M. sympodialis* and atipical *M. furfur*, meanwhile *M. pachydermatis* has been associated with the Kennedy pathway. Phospholipase C, responsible of forming DAGs, inositol and glycerol-3-phosphate has also been reported in different *Malassezia* species.[18,55] Also, genes encoding proteins involved in the ST biosynthesis and the generation of SE has been described for different *Malassezia* species. Acyl-CoA:cholesterol acyltransferases homologs were not found in *M. globosa.*[18] Even though this routes has been described, the differential association with consumption of specific lipids and their influence in these metabolic pathways remains to be determined.

LDs also participates in the membrane structure formation and regulation on energy homeostasis, energy storage, lipid metabolism, temporal protein storage, signal transduction, and even in the synthesis of molecules that mediate inflammation such as prostaglandin and leukotrienes.[13,43,56] All of these functions help the cells to buffer fluctuations in energy availability.[57] Lipid storage has been associated with the process of infection caused by different microorganisms. For example in viruses, specifically hepatitis C, LD mediate the assembly of viral particles and hepatic steatosis development.[58–60] Also, it has been described as a pathogenicity factor in different microorganisms such as *Mycobacterium tuberculosis* and associated with survival in species such as *Rhodococcus*.[61,62] LD versatility has sparked interest in study them, and yeasts have been used as a eukaryotic model to understand the biogenesis and metabolism of these organelles. In *M. furfur,* LDs have recently been reported*,* and its analysis revealed the presence of phospholipids and triglycerides.[12] It is speculated that LDs may play an essential role in *Malassezia* due to its lipid-dependent nature.[12]

Multiple approaches exist for LD studies. To investigate the distribution of LDs, morphology and growth dynamics *in vivo*, one widely used technique is confocal laser scanning microscopy.[63–65] In

comparison to traditional phase contrast microscopy, the confocal based-approach allows a superior depth sectioning, increase in resolution of images and 3-D reconstruction when needed. Image construction is carried out by placing a spatial pinhole at the confocal plane in front of the detector. This modification allow to eliminate ot-of-focus light, and increase axial resolution compared to a conventional wide-field microscope.[66] Two of the most common fluorophores for LD staining are Nile Red (NR) and BODIPY 493/503. However, LipidTOX has become an alternative used recently.[43,67–69] To observe the position of these organelles within the cell, double staining has been used. In the case of yeast, Calcofluor White (CW) has been one of the most used fluorophores for cell wall staining [1,70]. Other approaches used to assess the morphological and spatial characterization of LDs are coherent anti-strokes Raman spectroscopy and transmission electron microscopy.[43,47,49]

Other interesting approaches to characterize the composition of these organelles are omics studies, specifically lipidomics and proteomics. By using them, the composition and possible function of these organelles can be elucidated.[43,47,49,71] To achieve this analysis, extracting and purifying these organelles is a necessary previous step. Considering the variations in the cell wall and cell membranes among different organisms are needed to adapt protocols to fulfill the extraction and purification of LD.[43,69]

It is known that this yeast can modify the consumption of FAs to fulfill its biological requirements such as energy homeostasis, membrane biogenesis, signal transduction, among others.[2,5] Recently the first mass spectrometry-based lipidomics analysis of different species of *Malassezia* including *M. globosa* was performed by Celis Ramírez, A. M and collaborators.[18] TAGs, STs, DAGs, FAs, phosphatidylcholine (PC), phosphatidylethanolamine (PE), ceramides (Cer), cholesteryl ester (CE), sphingomyelin (SM), acylcarnitine (CAR), and lysophospholipids (LP) were the most common lipids among the species. Specifically, in *M. globosa*, diacylglyceryltrimethylhomoserine, and fatty acid esters of hydroxy fatty acids (FAHFAs) were found in a variable concentration. Cholesteryl esters (CE) were undetected in this specie.[18] Other Raman-based studies confirm differentiation among *Malassezia* species based on the detection of their lipid metabolic profile.[72] The present study demonstrates the differential utilization of lipid supplements among *M. globosa, M. pachydermatis*, and *M. sympodialis.*[72] The information provided in these studies opens the door to explore the role of lipids in the *Malassezia* life cycle.

Pathogenic mechanisms and secretory processes in microbes are closely associated as secretion virulence factors have been described for several prokaryotic and eukaryotic pathogens.[17,55,73] Specifically the secretion of proteins, lipids and even polysaccharides has been associated with pathogenicity in different yeast including *Cryptococcus neoformans* and *Histoplasma capsulatum*.[73–76] The production of extracellular vesicles carrying these virulence factors with the potential to modulate the host-pathogen interactions has been described for multiple yeast as a principal secretion pathway.[73] This mechanism has been also described for non-pathogenic yeast like *Saccharomyces cerevisiae*, implying that extracellular vesicles are not only related to pathogenicity, but may represent a eukaryotic solution to the problem of trans-cell wall transport.[73,77] This vesicles has been detected using centrifugation procedures designed for the purification vesicles, where the isolation of round vesicles lipid containing fractions were described.[73–75]

Analysis of extracellular lipid components in *Cryptococcus neoformans* revealed the presence of SL as glucosylceramides (GlcCer) and some ST such ergosterol and ergosterol derivates.[74] This molecules, specially GlcCer has been related with the pathogenicity of different fungi in plants and humans.[73,78,79] Additional, studies have shown that lipid microdomains consisting of glycosphingolipids and sterols might serve to concentrate virulence factors, modulating pathogenicity and infectivity.[78–80] In other hand, Sterylglycosides, ST derivates found in plants, algae and fungi also has been related to modulation in pathogenic response. This molecules has been described as important regulators of the host immune response to fungal infections.[79,81] However, there is still much to know on the role of lipids in fungal virulence. Within the lipid metabolism of *Malassezia*, previous reports have shown that oleic acid, a representative *Malassezia* FA, can induce scalp flaking in susceptible individuals. That study supports that *Malassezia* might be capable of FA-induced barrier disruption in patients.[82] This theory can be complemented with the role of other virulence factors such as azelaic acid, which is produced by *Malassezia furfur*, and associated with the develop PV phenotype.[83] Even though the secretion on different hydrolases and some virulence factors has been described, few has been reported about the lipid consumed and secreted composition and it´s possible role in the pathophysiology of *Malassezia* related diseases.

V. Problem statement

Given the relevance of *Malassezia* as part of normal microbiota and its multifaceted role, it is crucial to investigate lipid metabolism in *Malassezia,* its role in LD formation and the function of these organelles in the metabolism. Considering the abundance of *M. globosa* in human skin and its relation with multiple skin conditions, these species are of relevance to study. Although in *Malassezia furfur* LD were previously identified using a single staining procedure, double staining with fluorophores for LD such as NR, BODIPY 493/503, and LipidTOX deep red neutral has not been reported for this genus. Developing this procedure is helpful in order to determine both morphological and spatial information of this organelle within the yeast, based on the principle that double staining will allow to determine the position, size and number of LDs in each cell by combining the fluorescence images generated. Consequently, to understand the dynamics of LD and its role in lipid metabolism in *M. globosa*, the development of a double staining protocol is relevant. In other hand, the extraction and purification of LDs is a necessary step in order to delve in LD composition. Considering the variations in the cell wall and cell membranes among different organisms are needed to adapt protocols to *Malassezia* to fulfill the extraction and purification of LD.

On the other hand, recent studies have opened the door to new possibilities for deepening in *Malassezia* lipid metabolism to better understand this dynamic process. By determining the consume and the secreted lipids by *M. globosa*, a better insight into the factors that are involved in the multifaceted *Malassezia* behavior could be achieved. These approaches will allow complementing the information already known for this yeast lipid metabolism, giving valuable information regarding its dynamics.

VI. Objectives

1. General objective

To characterize the dynamics of lipid droplet formation in *Malassezia globosa* through the standardization of a double staining protocol using confocal microscopy and to characterize the consume and secreted lipids of this specie, to understand the lipid dietary composition and its relation with the environment.

2. Specific objectives

i. To establish a protocol for lipid droplets extraction in *Malassezia globosa.*

ii. To determine a double staining protocol using confocal laser scanning microscopy for the cell wall and lipid droplets in *Malassezia globosa*.

iii. To characterize the dynamics of lipid droplet formation of *Malassezia globosa* using confocal laser scanning microscopy.

iv. To characterize the specific classes of lipids consumed and secreted by *Malassezia globosa.*

VII. Materials and methods

1. Culture conditions for *M globosa*

The reference strain *Malassezia globosa* CBS 7966 (Westerdijk Institute, Utrecht, The Netherlands) was used for the whole study. A frozen stock was reactivated and precultured in modified Dixon (mDixon) agar (36 g/L mycosel agar [BD, USA], 20 g/L Ox Bile [Sigma Aldrich, USA], 36 g/L malt extract [Oxoid, UK], 2 mL/L glycerol [Sigma Aldrich, USA], 2 mL/L oleic acid [Sigma Aldrich, USA], and 10 mL/L Tween 40 [Sigma Aldrich, USA]) incubated at 33°C for seven days. Then, one colony was transferred to a new mDixon agar plate and was incubated for five days at 33°C. From this plate, colonies were taken up to a adjust an inloculum to standard of 2 on the McFarland scale in water plus 0.1% Tween 80 [Sigma Aldrich, USA]. From this suspension 3 mL was used to inoculate 27 mL of mDixon broth (36 g/L malt extract [Oxoid, UK], 6 g/L peptone [BD, USA], 20 g/L Ox bile [Sigma Aldrich, USA], 2 mL/L glycerol [Sigma Aldrich, USA], 2 mL/L oleic acid [Sigma Aldrich, USA], and 10 mL/L Tween 40 [Sigma Aldrich, USA]) for 96 hours at 33°C and 180 rpm. An aliquote of 300 μl was used to inoculate 29.7 mL of fresh mDixon broth and incubated at 33°C and 180 rpm. A flask with fresh mDixon was used as a sterility control for each experiment. The incubation time was different for each experiment (**Table 1**). A growth curve previously determined by Grupo de Investigación Celular y Molecular de Microorganismos Patógenos (CeMoP) research group, was used as reference to determine the different growth phases used in this study.

Table 1. Time of growth required to reach different growth phases for *M. globosa*

Time of growth (hours)	Growth phase according to the growth curve
24	Lag phase
30-60	Exponential phase
72	Early stationary phase
90-96	Stationary phase
108	Late stationary phase

2. Lipid Droplets extraction

a. Solutions and buffers

The following solutions were used to perform LD extraction: Enzyme buffer: lytic enzymes of *Trichoderma harzianum* [Sigma Aldrich, USA] at 16 mg/g wet weight of yeast in 600 mM $(NH_4)_2SO_4$

[Sigma Aldrich, USA] pH 5.6. Solution I: 400 mM sucrose [Sigma Aldrich, USA], 10 mM Tris [Sigma Aldrich, USA], 1 mM EDTA [Sigma Aldrich, USA] at pH 7.0. Buffer A: 10 mM MESTris [Sigma Aldrich, USA] pH 6.9, 12% Ficoll 400 [Sigma Aldrich, USA], 0.2 mM EDTA [Sigma Aldrich, USA], and 1 mM phenylmethylsulfonyl fluoride (PMSF) [AMRESCO, USA]).

b. Lipid Droplet extraction procedure

LDs extraction was performed using a previous protocol standardized for *M. pachydermatis* and other reports.[84,85] Briefly, 30 mL of cultured yeast were used at the early stationary phase. The culture was washed three times with phosphate buffer saline (PBS) at pH 7.4 by centrifugation at 4,500 g for 5 minutes. Then, the enzymatic digestion of the cell wall was performed using 10 mL of enzyme buffer. Cells were incubated in the presence of lytic enzymes in a shaking incubator at 47°C and 52 rpm for 18 hours. Then the cells were washed twice with a solution I.

Mechanical disruption was needed to disrupt the cell wall completely. Cells were recovered at 3,000 g for 5 min and resuspended at a ratio of 1 mL/g wet weight of yeast in buffer A. 0.92 g of 0.5 mm zirconium beads were added to the resuspended cells and vortex for 1 minute followed by incubation on ice for 30 seconds. This procedure was repeated 50 times. Afterward, cells were stroked 120 times with a Dounce homogenizer with a loose-fitting pestle. Finally, the homogenate was diluted with 0.5 volumes of buffer A and centrifuged at 6,000 g for 10 minutes. The supernatant containing LDs was stored at 4°C.

Evaluation of the LDs extraction procedure was done by two methods. 1) yeasts were growth before the enzymatic lysis and after the mechanical disruption mDixon agar at 33°C for 7 days. If the process was carried out efficiently, the integrity of the cell wall was compromised and reflected by a minor growth of the yeast. 2) confocal microscopy with NR and CW was used to determine the spatial location of LDs before and after the extraction procedure. Also, this method allows to observe the differences and possible effects on the cell wall based on the intensity of the fluorophore CW in processed images.

3. Confocal microscopy imaging

a. Stocks solutions

The following stocks were used for this study: 1 mg/mL Nile Red [Sigma Aldrich, USA] in methanol (MeOH), 0.1 mg/mL BODIPY™ 493/503 [Invitrogen, USA] in MeOH, 100X HCS LipidTOX™ Deep Red

Neutral [Invitrogen, USA] in DMSO, 0.01% Calcofluor White [Sigma Aldrich, USA] in water and KOH 10% (m/v) in water.

b. Staining procedure

Staining standardization was performed for the three fluorophores (NR, BODIPY™ 493/503 and HCS LipidTOX™ Deep Red Neutral) in *M. globosa* cultures grown at 72 h and 108 h based on previous reports.[63,86–88] Cultures were washed three times with phosphate buffer saline (PBS) at pH 7.4 using centrifugation at 5,000 g for 5 minutes. Afterward, cells were resuspended in 0.1 mL of paraformaldehyde 4% (v/v). Then 2 μL of each fluorophore solution was added, and cells were incubated in continuous darkness for 2 hours at 30°C and 52 rpm in an incubator shaker. Then, cells were washed twice with 200 μL of PBS at 1300 g for 3 minutes, resuspended in 100 μL of 4% paraformaldehyde and homogenized. To assemble the microscopic slide, 2 μL of previous preparations, 2 μL of CW solution, and 2 μL of 10% KOH were added.

The images were taken at μ-core at Universidad de los Andes (https://microcore.uniandes.edu.co/es/) using an Olympus FV1000 confocal laser scanning microscope with a 60X / 1.42 NA oil immersion objective. Each microscope image was taken as a stack of 18 to 25 images with a stack thickness of 0.5 and a digital zoom of 2X unless otherwise stated. Different filter parameters were used for imaging with the different fluorophores (**Table 2**).

Table 2. Microscope parameters used for imaging with different fluorophores.

Fluorochrome	Microscope filter	Excitation (nm)	Emission (nm)
Nile Red	Alexa 488	488	545
BODIPY 493/503	FITC	493	503
LipidTOX Deep Red Neutral	Alexa 633	637	655
Calcofluor White	DAPI	365	440

c. Lipid droplets growth dynamics curve

Aliquots from *M. globosa* in culture were taken at 24 h, 48 h, 72 h, 90 h, 96 h and 108 h. NR staining was used for curve construction. A total of 100 cells per hour were counted. The total area of each cell was measured along with the number of LD inside it. Then for each LD the area and circularity were determined. In this case, circularity was measured in a range from 0 to 1, where 1 indicates a

perfect circle (equation 1). These analyses were performed using the Fiji image processing package of Image J2 (www.fiji.sc). All areas were measured in μm^2 and were used to calculate the area percentage of the cell occupied by LDs (equation 2). These data were used to perform a violin analysis using R version 4.0.0 (https://www.rstudio.com/) with the ggplot2 library.

$$\text{Circularity } = 4\pi * \frac{(\text{Area of LD})}{(\text{Perimeter of LD})^2} \ (\boldsymbol{Eq.1})$$

$$\%\ \text{LD area} = \frac{\text{Total LD area}}{\text{Yeast area}} * 100 \ (\boldsymbol{Eq.2})$$

4. Determination of consumed and secreted lipids by *M. globosa*

    a. Growth conditions and experimental design

In this experiment two treatment groups were established. One group consists of yeast growth at 72 hours and the other growth at 90 hours. From both groups, *M. globosa* supernatant was analyzed. Experiments for these groups were performed in hexaduplicates. Additionally, three different control groups were established. The first one consists on a mDixon fresh broth. The other two were the *M. globosa* pellet at 72 h and 90 h. Experiments for each control were performed by triplicate.

Briefly, a single overnight culture of *M. globosa* was used to inoculate twelve different Erlenmeyer flasks. Six of these flasks were growth for 72 h at 33°C and 180 rpm, and the other six were growth up to 90 h at the same conditions. Additionally, four flasks containing fresh mDixon were placed in the same conditions as controls. Three of these mDixon flasks were used as the media control for the experiment, and the fourth one was used as sterility control throughout the whole experiment.

    b. Lipid extraction of *M. globosa* supernatant collection

Samples of 72h and 90h treatment groups were centrifuged at 4,500 rpm for 10 min, and supernatants were collected. Then, 5 mL of isopropanol was added to the supernatant and centrifuged at 4,500 rpm for 10 min. Lipid extraction was performed according to Bligh and Dyer lipid extraction with some modifications.[61,89,90] Briefly, 2mL of a citric acid buffer (100 mM sodium citrate tribasic dihydrate, 1 M sodium chloride, pH 3.6, 2 mL of MeOH and 4 mL of chloroform were added to 8 mL of supernatant collected previously. The mixture was homogenized with vortex for 15 min and sonicated for 30 min. The organic phase containing the extracted lipids was collected and dried on a Speed Vac. Then, the dry extract was re dissolved in 1 mL of Acetonitrile (ACN) containing 0.1% NH3·H2O (v/v), followed by strong anion-exchange solid-phase extraction using

Strata SAX SPE-cartridge (55 uM, 70 A, 100 mg, 1 mL Phenomenex) which was pre-conditioned with 3 mL ACN. After sampling 1 mL of the lipid extract, the cartridge was washed with 3 mL acetone/H2O (1/9, v/v), 3mL acetone, and eluted with 3 mL formic acid/acetone (1/99, v/v) followed by evaporation using a Speed Vac. Samples were stored at -80°C for one week and dissolved in 1 mL of MeOH for further analysis.

c. Lipid fingerprinting HPLC-QTOF analysis

Lipid analysis was performed by the MetCore at Universidad de los Andes (https://metcore.uniandes.edu.co/es/) using a Agilent Technologies 1260 HPLC coupled with a qTOF 6545 with electrospray ionization. A dilution 1:100 was necessary prior injection. MeOH used to dissolve the samples were used as the blank of the method. 1 µL of the samples were injected onto an InfinityLab Poroshell 120 EC-C18 column (100 x 3.0 mm, 2.7 µm). Chromatographic analysis was carried out at 65°C and constant flow 0.6 mL/min using gradient elution with phase A (60:40 Acetonitrile : type I water with 10 mM of ammonium formate and 0.1% v/v of formic acid) and mobile phase B (90:10 Isopropanol : Acetonitrile with 10 mM of ammonium formate and 0.1% v/v of formic acid). Gradient conditions are show in **Figure 7**.

Time (min)	Phase B (%)
0	15
4	30
5	48
22	82
23	95
25	95
26	15
31	15

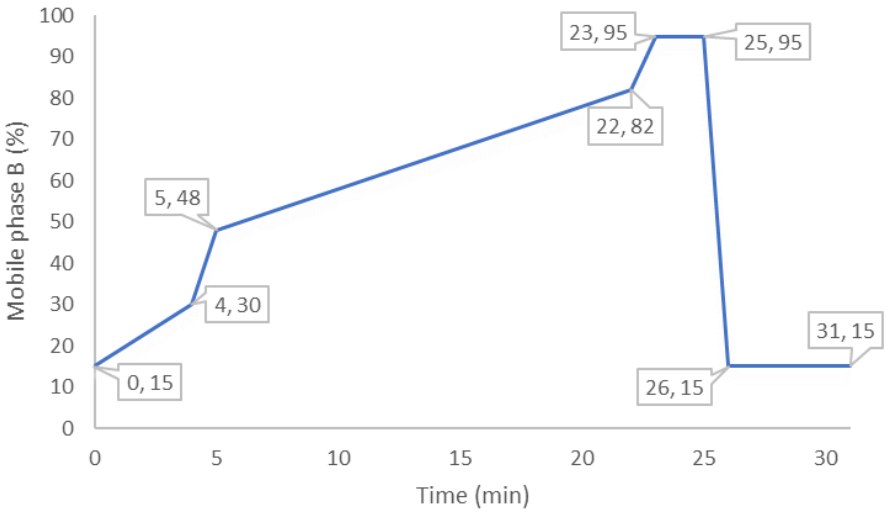

Figure 7. Chromatographic gradient conditions used in the sample analysis.

Mass spectrometry detection was performed in positive ionization mode in a full scan from 100 m/z to 1200 m/z. During the analysis, the mass correction was performed with reference masses: m/z 121.0509 ($C_5H_4N_4$) y m/z 922.0098 ($C_{18}H_{18}O_6N_3P_3F_{24}$). Mass spectrometry conditions are shown in.

Table 3.

Table 3. Mass spectrometry parameters used in lipid fingerprinting

Fuente – Dual AJS ESI	
Vcap (V)	3500
Drying Gas (L/min)	8
Gas Temp (°C)	325
Nebulizer (psi)	35
Sheat Gas Temp (°C)	350
Sheat Gas Flow (L/min)	11
MS TOF	
Fragmentor (V)	120
Skimmer (V)	65
OCT RF Vpp (V)	750

d. Data processing

Profiles obtained were deconvoluted and molecular characteristics identification were aligned according to its mass and retention time using the software Agilent Mass Hunter Profinder 10 via the algorithm Recursive Feature Extraction (RFE) with the following conditions: Extraction from 0-25 minutes and minimum 10,000 counts. Ions species considered in this analysis were: -H, +Cl, $+NH_4$. No additional filters were used. Data matrices were imported into Microsoft Excel (Microsoft Office 2016). Each molecular characteristic was manually processed, and those present in the blank were eliminated.

d. Quality control samples.

Quality control (QC) samples were prepared mixing a pool of equal volumes of all the treatment group samples (72 h and 90 h). Reproducibility of sample preparation and the stability of the analytical platform was assessed by running the QC multiple times until the system was stabilized. QC samples were injected every five aleatory samples. For data processing, molecular features, were identified as a specific mass related to a retention time. Data was filtered based on the coefficient of variation (CV) of the metabolite levels in the QCs, a threshold of 20% was established.

e. Statistical analysis

Univariate (UVDA) and multivariate (MVDA) statistical analyses were performed to investigate differences among the molecular features detected in the mDixon control group, and the two treatment groups (72 h and 90 h).

For UVDA, normality of data was evaluated with the Shapiro-Wilk test ($p \leq 0.05$). Wilcoxon test ($p \leq 0.05$) were performed to the following pairings: 72 h vs 90 h, 72 h vs mDixon and 90h vs mDixon to evaluate differences for an individual metabolite in each of the three pairings. Additional, differences among the three groups was evaluated by performing a non-parametrical Kruskal-Wallis test ($p \leq 0.05$). Posthoc, pair-wise analysis was performed using the Dunn test to conclude for which group the metabolite present a significand difference. Finally, the false discovery rate at level $\alpha = 0.05$ for all UVDA analysis were controlled by Benjamini–Hochberg correction test. All UVDA analysis was performed using R version 4.0.0 (https://www.rstudio.com/).

For MVDA, unsupervised (PCA, principal component analysis) and supervised (PLS-DA partial lest-squares discriminant analysis and OPLS-DA, orthogonal PLS-DA) models were performed. These analyses were performed to determine differences in molecular features intensity between groups. All models were evaluated by the explained variance (R2) and the predicted variance (Q2) quality parameters. Additionally, the Variable Importance Parameter (VIP) ≥ 1 and jackknifing confidence interval not including zero were selected as statistically significant from the OPLS-DA models. All the analyses were performed in SIMCA 14.1. Additionally, a heat-map graphical representation of the differential lipid expression of the detected lipids was performed using R version 4.0.0 (https://www.rstudio.com/). This map displays the relative differences in intensities observed for the same molecular feature in the two treatment samples and mDixon control.

f. Lipid annotation

A tentative identification based on the m/z of the compounds showing significant differences were searched against several databases available online such as METLIN (https://metlin.scripps.edu), lipidsMAPS (http://lipidmaps.org), HMDB (https://hmdb.ca/), and KEGG (https://www.genome.jp/kegg) using the search engine, CEU MassMediator (http://ceumass.eps.uspceu.es/mediator). Molecular features assigned to metabolites from the databases were based on mass accuracy (maximum error mass of 20 ppm). Molecular features were also inspected with the Agilent MassHunter Qualitative Analysis Software B.10.00.

VIII. Results and discussion

1. Lipid Droplet extraction procedure

The process of disrupting the cell wall without damaging organelles is a critical point in LDs extraction and purification processes.[43] In other organisms such as mammalian cells, bacteria, and yeast, several methodologies have been used: enzymatic, chemical, or mechanical lysis to achieve this extraction.[69,91,92] In this protocol, enzymatic lysis followed by mechanical disruption was necessary to open the cell wall.

Trichoderma harzianum lytic enzymes (1,3-β-glucanases and chitinases) were used in the first stage of the protocol.[93] It is known that *Malassezia* cell wall is constituted by linear β-(1,6)-glucan chains with β-(1,3)-glucosyl chains as branches that appear every 3.8 glucose unit, making β-(1,6)-glucans the most abundant glucan in these yeasts.[70] For *Malassezia,* 18 hours of enzymatic digestion were necessary while in other fungi like *Ustilago maydis*, 45 minutes of the reaction was enough to generate the cell wall rupture.[85] This observation can be explained by the low percentage of β-(1,3)-glucans and chitin. [70] Also, the cell wall thickness and multilamellar form can add extra time to fulfill an enzymatic lysis.[70,94]

To prevent degradation or proteins associated with LDs, the buffer used for mechanical disruption contained a protease inhibitor phenylmethylsulfonyl fluoride (PMSF).[95] This is a serine protease inhibitor that acts by sulfonation of the γ-oxygen atom of the serine residue in hydrolases catalytic side, obliterating the active site and leading to irreversible inhibition of catalytic activity.[96] Mechanical disruption was carried out using zirconium beads. This procedure has been used in order to obtain protoplasts several species including algae and yeast.[31,63,97]

Three methods evaluated the cell wall rupture. First was on the mDixon agar culture plate, where the disruption was assessed by observing the decrease in cell viability after the extraction procedure. The second method was the double staining of cells with NR and CW. Through this experiment was possible to observe the affected cell wall based on the intensity of the signal emission of CW. The decrease in intensity was directly associated with the loss of the cell wall integrity, translated to less chitin and glucans for CW to stain. The third method was gram staining performed on cells before and after the extraction procedure (data not shown). It was observed that the color of the cell

turned from a deep purple to a lighter purple, sometimes pinkish color after the extraction was completed. This was directly associated with the disruption of the cell wall or cell wall thinning.

To continue with the extraction protocol, a 30X cycle of the vortex with zirconium beads followed by ice cooling intervals was used. This protocol has been effective in *M. pachydermatis,* but only partial cell wall disruption was achieved in *M. globosa* (Data not shown). As mentioned before, this can probably be attributable to the differences in the cell wall; some authors have described *M. globosa* and other *Malassezia* species.[1,94] The number of mechanical lysis cycles was increased to 50X. This increment proved to be effective, showing a complete cell wall disruption for *M. globosa* (**Figure 8**). The early stationary phase was selected to perform this experiment based on the LD dynamics were at 72 hours a high proportion of the cell have LDs.

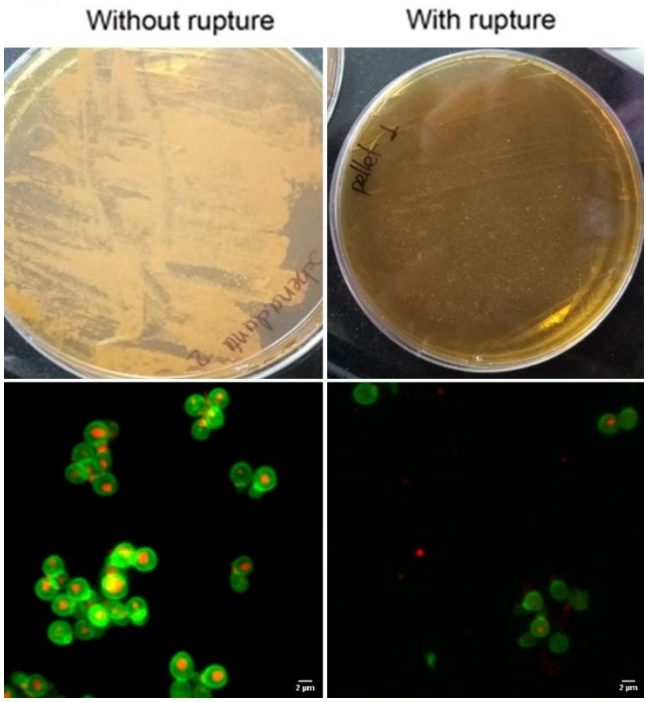

Figure 8. Evaluation of the rupture in *M. globosa* cell wall by **A)** culture in mDixon agar and **B)** co-staining between Nile red (red) and calcofluor white (green). The figure on the left side is the control without any mechanical or enzymatic disruption. Scale bar 2µm

After the extraction of LDs was achieved, confocal microscope images showed some impurities (**Figure 9**). Based on LDs low density, purification procedures with ultracentrifugation have been proposed.[69] For correct recovery of these organelles, the speed is critical and depends on LDs size. If these organelles are large, high speeds could disrupt them or stick them to other cell components. However, if speed is slow, small LDs can be lost. For this case, a preliminary ultracentrifugation procedure was used as an alternative. Briefly, cells were centrifuged at 182,000 g for one hour, and

the top layer was observed by confocal microscopy, showing some cellular residues (Data not shown). A replica of the purification should be done.

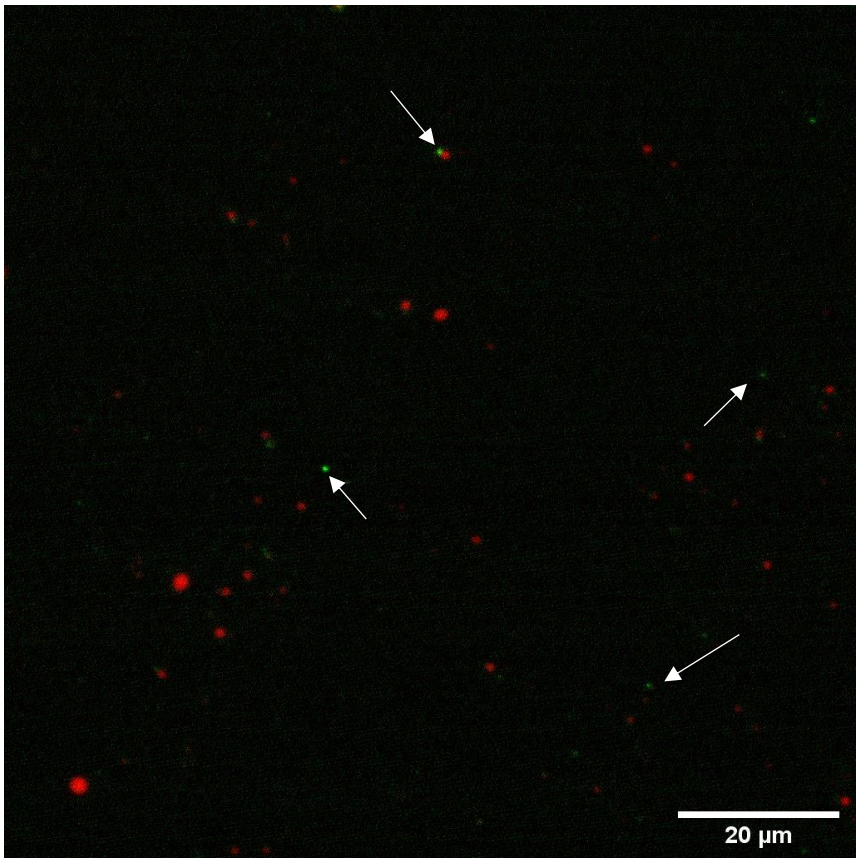

Figure 9. Lipid droplets supernatant with after extraction procedure. Scale bar 20µm. Zoom 1X. White arrows denote the cell wall residues observed.

2. Fluorescent double-label staining protocol standardization.

Standardization of a double staining protocol for LDs and cell wall detection in *M. globosa* was achieved using three different fluorophores: NR, BODIPY 493/503, and LipidTOX deep red neutral using CW for cell wall staining. Fluorophore double staining protocols were adapted from protocols previously performed in *Malassezia* spp., and other yeasts.[13,87,88]

CW was chosen for cell wall staining based on two principles. First, it is a well-known fluorophore used for stain yeast cell walls.[98,99] The mechanism of action relies on its highly planar structure, a derivative of stilbene that associates with straight-chain polysaccharides containing free hydroxyl groups (**Figure 10**).[100] It is known that CW can bind glucan chains through hydrogen bonding and dipolar interactions. However, its structural conformation generates a preference of binding toward β(1-3) and β(1-4) linkages present in chitin and cellulose.[101] Second; this is a blue-emitting

fluorophore (λ_{em} < 500 nm) having an excitation around 365 nm and an emission spectra peak around 440 nm, which prevent spectra overlapping with the other fluorophores used in this work, whose are considered green dyes (λ_{em} = 500-550 nm) and red (λ_{em} > 600 nm) emitting fluorophores (**Table 2**).[65,102] KOH was added to enhance fungal visualization clearing possible cellular residues.[99]

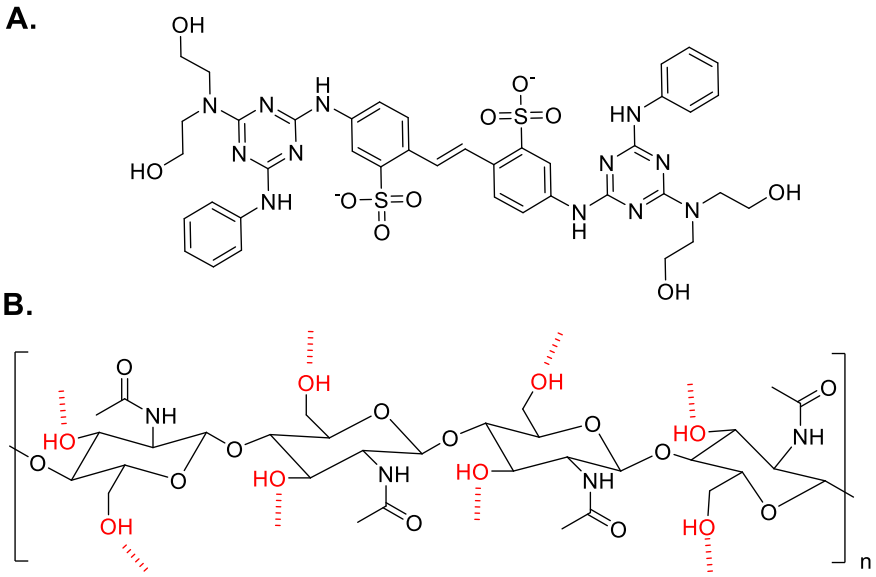

Figure 10. Structure and interaction sites of Calcofluor white. **A.** Calcofluor White structure. **B.** Beta-chitin showing 1-4 glucan linkages. In red are shown free hydroxyl groups which interact with Calcofluor White.

NR dye was selected because it is a widely used, well known, easy-to-handle fluorophore in LD detection in multiple organisms including mammalian cells, parasites, yeast and bacteria among others.[65,87,103–105] This fluorophore is a benzophenoxazone dye with known solvatochromic properties generated by a robust solute-solvent interaction (**Figure 11A-B**).[106] With proton donor solvents such as EtOH, the solvent interactions are primarily hydrogen bond meanwhile π-staking, and other hydrophobic interactions rule towards less polar solvents such as toluene.[106] In general, this fluorophore has a bathochromic shift and an increase in intensity emission when it is dissolved in less polar solvents.[65,103] The affinity of NR for lipophilic environments allows the target of lipid storage organelles such as LDs, which polarity is different from other cell components such as cytoplasm. NR staining procedure was standardize based on a protocol reported for single staining in *M. furfur*[12] with the following modifications*:* water was replaced for MeOH as solvent, as it shows more consistent results. The incubation time and temperature were increased up to two hours and 30°C. [103,104,107] The standardization of double staining procedure with CW was achieved by lowering the concentration of CW to 0.1% m/w with no further modifications on the staining procedure for NR.

On the other hand, BODIPY 493/503 and HCS LipidTOX Deep Red Neutral were chosen to corroborate LD presence in *M. globosa* because these fluorophores are known to be specific towards LDs and neutral lipids.[65,107] BODIPY 493/503 a dye with a small structure allows relatively fast diffusion through membranes (**Figure 11C**).[108] Also, the hydrophobicity of BODIPY 493/503 facilitates rapid uptake by intracellular LDs.[109] For LipidTOX Deep Red Neutral, there is no published structure, and there is little known about its mechanism of action.[110]

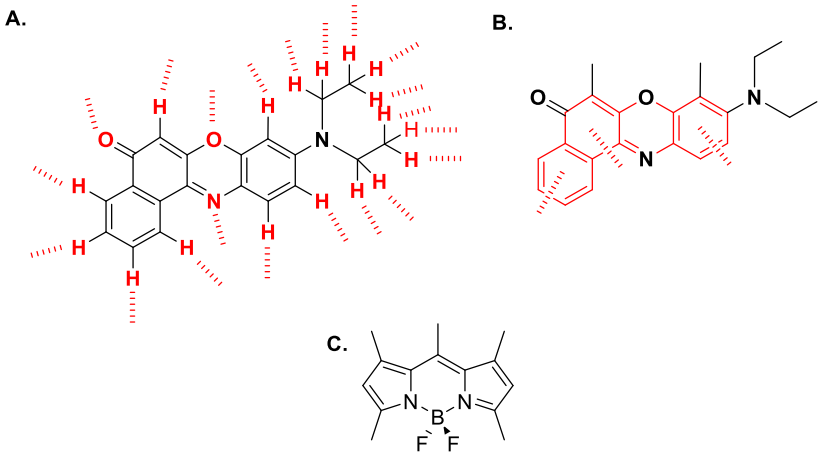

Figure 11. Nile red and BODIPY 493/503 structure. **A.** Nile Red structure and visualization of its principal interactions with protic polar solvents. **B.** Nile Red structure and visualization of interactions with aprotic nonpolar solvents. **C.** BODIPY 493/503 structure

BODIPY 493/503 staining process was performed based on the evidence that the cell wall of the *Malassezia* genus is unique among yeast species, as evidenced in the LDs extraction procedure. This cell wall is described as thick and multilamellar, which probably affects the permeation rate of fluorophores through the cell wall.[70,111] Based on this information, the incubation time, solvent, fluorophore concentration, and fixation-incubation time were modified and tested to get an efficient process to stain *Malassezia* using this fluorophore. First, a single staining procedure was performed using two different dilutions of final stock concentration of 1 mg/mL and 0.1 mg/mL in two different solvents, EtOH and PBS (**Figure 12**). The fixation of all the cells was performed with a solution of PFA 4% before cells were incubated. The protocol used for the staining procedure was based on previous protocols, where the cell was fixated with a solution of PFA of 2% m/v to 4% m/v. Then incubation was performed for 10 min with BODIPY 493/503 at a stock concentration of 1.25 mg/mL to 1mg/mL.[67,87,88,112]

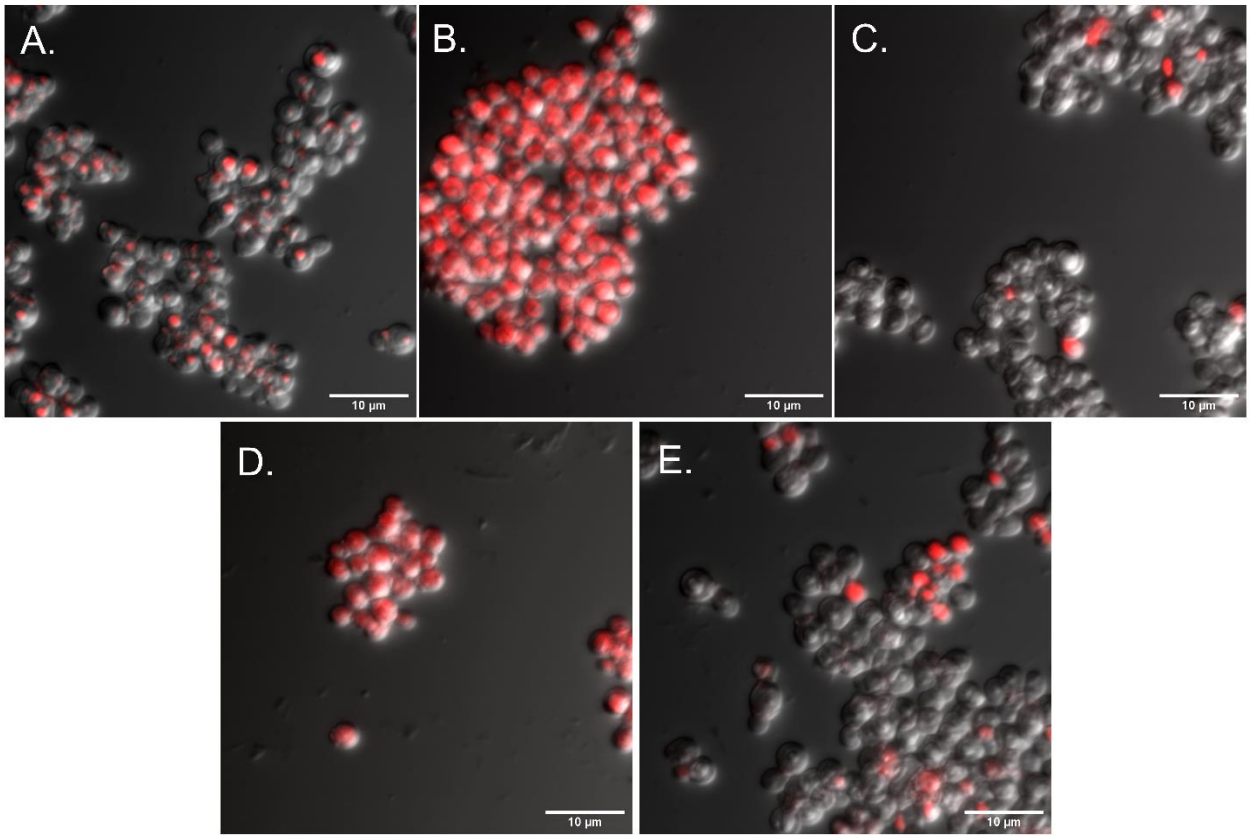

Figure 12. The stain of Lipid droplets for *M. globosa* CBS7966 with the following solutions **A.** Nile Red LD. **B.** 1.0 mg/mL of BODIPY 493/503 in EtOH **C.** 1.0 mg/mL of BODIPY 493/503 in PBS **D.** 0.1 mg/mL of BODIPY 493/503 in EtOH **E.** 0.1 mg/mL of BODIPY 493/503 in PBS

EtOH showed more homogeneous results than PBS in the staining procedure. However, neither of the experiments (BODIPY-EtOH) or (BODIPY-PBS) was able to label LDs as NR. It was observed a deficiency in the permeability of the fluorophore through the cell wall and/or cell membrane. This is attributable to the highly lipophilic structure, which probably agglomerates in aqueous media. No differences between the two dilutions were observed. Further experiments were carried out to standardize BODIPY staining with 0.1 mg/mL. First, the fixation procedure with PFA was modified, with no visible improvements on the method. (**Figure 13**).

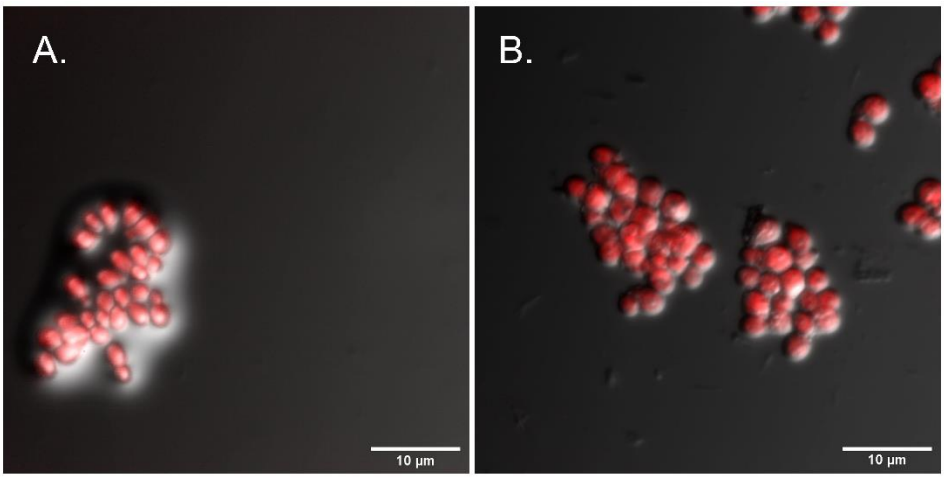

Figure 13. The stain of Lipid droplets for *M. globosa* CBS7966 with the following solutions **A.** 0.1 mg/mL of BODIPY 493/503 in EtOH with fixation with PFA 4% before incubation **B.** 0.1 mg/mL of BODIPY 493/503 in EtOH with fixation with PFA 4% after incubation

Afterward, the incubation temperature and incubation time were further modified to increase the permeability rate. Based on the results obtained with the control dye NR, the solvent was changed from EtOH to MeOH, and the incubation time and temperature were increased to 2 hours at 30°C. As a result of these modifications, BODIPY 493/503 staining procedure was standardized for *M. globosa.* (**Figure 14** - **Figure 15**). This procedure was later tested in *M. pachydermatis* with favorable results, hinting this protocol might be useful in different species of *Malassezia* genus. (Data not shown).

The double-staining protocol was tested in triplicates throughout the stationary phase considering that the cell wall changes its thickness as the time progresses, becoming harder as they get older. Also, considering the permeability problems faced before, this was done to assure that the protocol will work throughout the lifespan of the yeast.

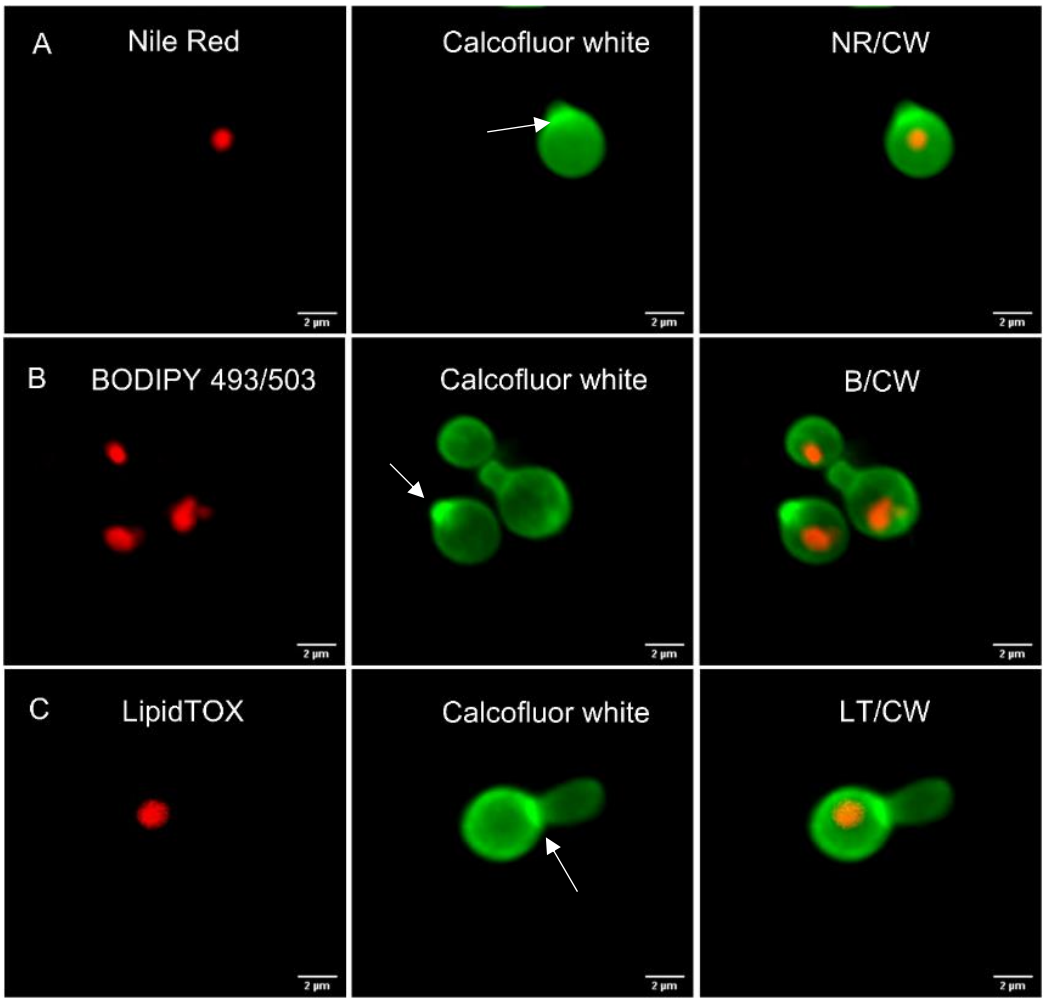

Figure 14. Co-stain of Lipid droplets and *M. globosa* CBS7966 after 72 hours of incubation (early stationary phase), with the following stains: **A.** Nile Red (NR - red) and calcofluor white (CW - green). **B.** BODIPY 493/503 (B - red) and calcofluor white (CW - green). **C.** LipidTox deep neutral red (LT - red) and calcofluor white (CW - green). White arrows denote a higher intensity of Calcofluor White in budding scars. Scale bar 2 µm. Zoom 4X.

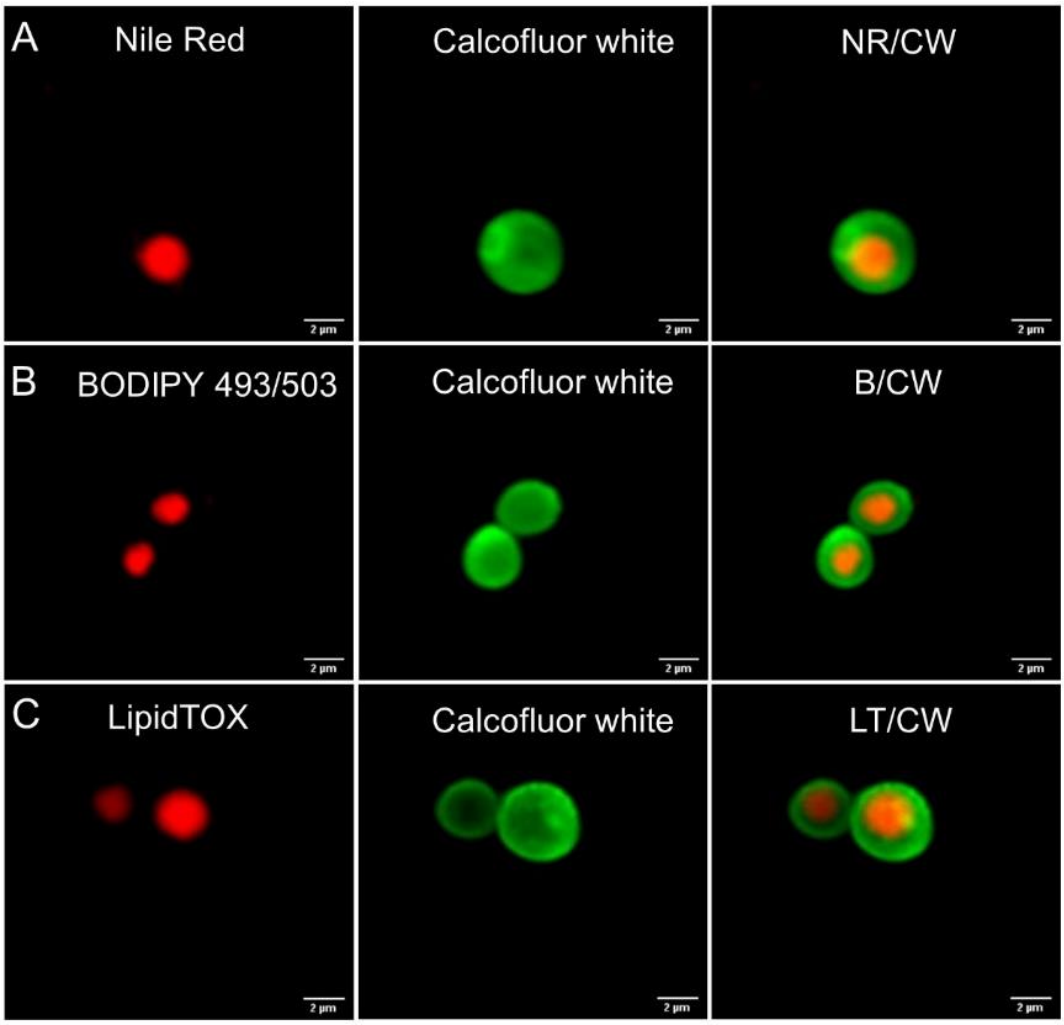

Figure 15. Co-stain of Lipid droplets and *M. globosa* CBS7966 after 108 hours of incubation (late stationary phase), with the following stains: **A.** Nile Red (NR - red) and calcofluor white (CW - green). **B.** BODIPY 493/503 (B - red) and calcofluor white (CW - green). **C.** LipidTox deep neutral red (LT - red) and calcofluor white (CW - green). White arrows denote a higher intensity of Calcofluor White in budding scars. Scale bar 2 µm. Zoom 4X.

It is shown that regardless of the growth time of the yeast, it was possible to visualize LDs using the three combinations of double staining procedures. CW was the right choice for staining the *M. globosa* cell wall, showing reproducible results independent of the fluorophore used for LDs co-staining (**Figure 14** - **Figure 15**). Also, the concentration of the fluorophore was adequate for double fluorescence imaging, and no spectra were overlapping between CW and NR, BODIPY 493/503 or HCS LipidTOX Deep Red Neutral. Additionally, it is observed that near to the budding scars, there is a higher fluorescence intensity for CW (**Figure 14**). This is related to the fluorophore's affinity to chitin, which is restricted to the region of bud scar formation in some *Malassezia* species.[1,113]

Now, compared to other fluorescence staining methods reported for yeast such as *Saccharomyces cerevisiae* and *Rhodotorula minuta*, concentrations of fluorophores and fixation agents used were similar to reported ones.[63,86,87,114] However, incubation time and, in some cases, incubation temperatures for the three fluorophores were significantly higher than the ones used in another genus. This can be attributed to the unique characteristic of thickness and multilamellar cell wall in *Malassezia* genus which is probably affecting fluorophores permeation rate.[70,94]

NR staining procedure in *M. globosa* was a simple experimental method, regardless of some drawbacks reported in the literature, such as non-specific labeling of lipid organelles and broad emission and excitation spectra that could have compromised the double staining procedures.[65] Experimentally, no overlap in the emission ranges of fluorophores was observed. This was evidenced based the low signal observer from the NR on the filter used to read CW signal. MeOH was used as a solvent, and its polarity helps the selectivity of this dye. Similar fluorophore selectivity was noted for the three staining experiments.

Although BODIPY™ 493/503 LD imaging showed good organelles definition, demonstrating a good selectivity and resolution, the biggest problem with this dye is the photobleaching observe at the same time, images were taken, hindering the experimental detection of LDs.[65,115,116] Usually, adding an anti-quencher reagent during the staining procedure and minimizing light exposure helps to overcome this drawback.[64] However, these solutions can increase experimental cost and requires more considerable precautions at the experimental level. Interestingly, BODIPY™ 493/503 showed less photobleaching effect when dual staining was performed. This is probably attributable to the pH change from acid to basic when KOH is added, therefore stabilizing the structure.[117]

On the other hand, HCS LipidTOX Deep Red Neutral double staining displays a similar selectivity as NR and BODIPY™ 493/503. However, LDs images obtained showed lower resolution compared with NR and BODIPY™ 493/503 staining, especially at 72 h. This pattern was also observed in *M. pachydermatis* (Data not shown). This is due to staining problems of HCS LipidTOX Deep Red Neutral into smaller LDs, as reported before.[118] Also, previous studies reported the lacks of the stability of this fluorophore experimentally, possibly this and the non-complete permeation through *Malassezia* thick cell wall could be possible causes of the data obtained.[70,119]

Considering experimental and imaging drawbacks observed for BODIPY 493/503 and HCS LipidTOX Deep Red Neutral, NR dual staining was the most straightforward and uncomplicated procedure to stain *M. globosa.* For BODIPY 493/503, the photobleaching problem hindered image taking,

especially stacks, and for LipidTOX Deep Red Neutral image, lower resolution affected the image quality. Regardless of the issues observed, it was possible to detect the presence of LDs in *M. globosa* with laser scanning confocal microscopy using a combination of these fluorophores.

3. Lipid Droplet dynamic curve using confocal microscopy

M. globosa LD dynamics were studied qualitatively and quantitatively for 108 h, covering different stages of yeast growth. As LDs are highly dynamic organelles, during various stages of growth, their morphology and size vary.[49,120] From qualitative analysis, it was observed that LDs appears at 48 hours of growth (**Figure 16**), suggesting that their formation starts in the exponential phase. It is known that in yeasts, the synthesis of TAGs, molecules related to LDs biosynthesis begins during the exponential period. The synthesis of TAGs occurs primarily through the activity of the *LRO1*-encoded enzyme, which has been reported in *M. globosa*.[18,121] Although this can be directly related to the dynamic observed for LD formation, further analysis within 24 h and 48 h are recommended to get a better understanding of LD formation in this species.

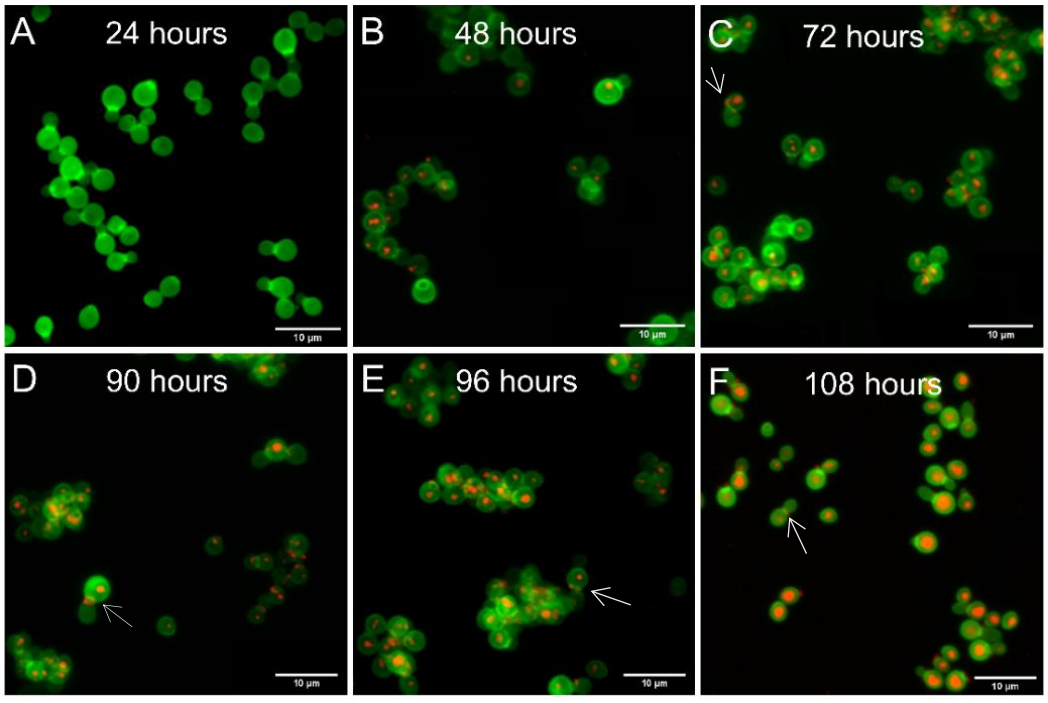

Figure 16. Co-stain of Lipid droplets and *M. globosa* CBS7966 with Nile Red (red) and calcofluor white (green) in the following hours of incubation **A)** 24h. **B)** 48h. **C)** 72h. **D)** 90h. **E)** 96h. **F)** 108h. White arrows show coalescence of Nile Red observed in budding scars. Scale bar 10µm

The qualitative analysis performed to LD also revealed that when yeasts were entering to stationary phase, an accumulation of the dye NR started to appear towards the budding scars of the cells. In

other yeasts, LDs are critical for the maintenance of membrane homeostasis.[15,122] This result suggests that LDs may be related with *Malassezia* budding process. In other yeast, LDs has been associated with the delivering of building block for membrane synthesis of daughter cells.[49] There was also evidence that LD is not necessarily transferred to daughter cells, as daughter cells with no LD were observed. Usually, yeast cells missing LDs were smaller, evidenced clearly in the early and late stationary phase (**Figure 17**). For budding cells, the transfer process was not evidenced in all stages of growth, both budding cells with and without LDs were observed.

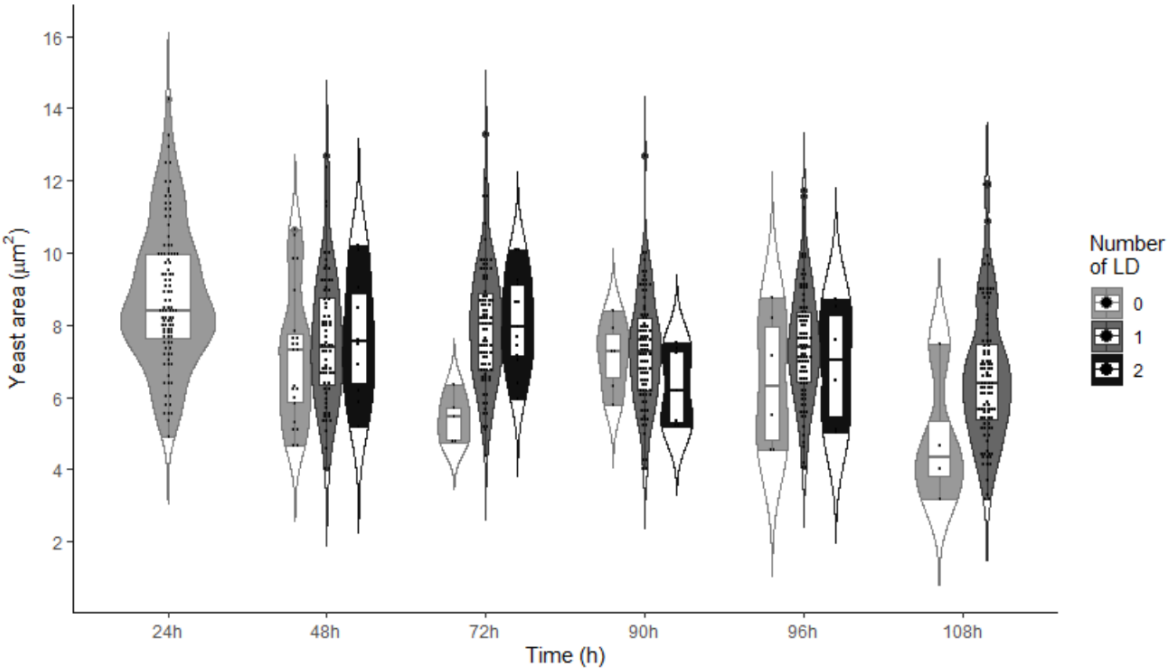

Figure 17. Analysis of the number of LD per cell (grayscale) and the yeast area (y-axis) of *M. globosa* in different hours of growth (x-axis).

During the exponential and early stationary phase, some yeast cells displayed two LDs, but in later growth stages, no yeast with two LDs was observed. This pattern was confirmed quantitively, where at latter stationary phases, the number of yeasts with two LD decreased towards 108 hours (**Figure 18**). Also, LD size increased while yeast reached later stationary phase, ranging from approximately 0.5µm^2 to 1.5µm^2 in exponential growth phase up to 1 µm^2 to 6µm^2 in late stationary phase (**Figure 19**). It is interesting to note that not only size increases but variation among LDs size also increases. The diameter of *M. globosa* LDs was around 0.4 and 1 µm with some bigger LDs up to 1.4 µm. The size of LDs observed was in the range of those reported in other yeasts ~ 0.65 µm to 2.5 µm for *Y. lipolytica* and 0.5-0.4 µm for *S. cerevisiae* with some few larger droplets with a diameter of 1.2–1.6 µm.[123,124]

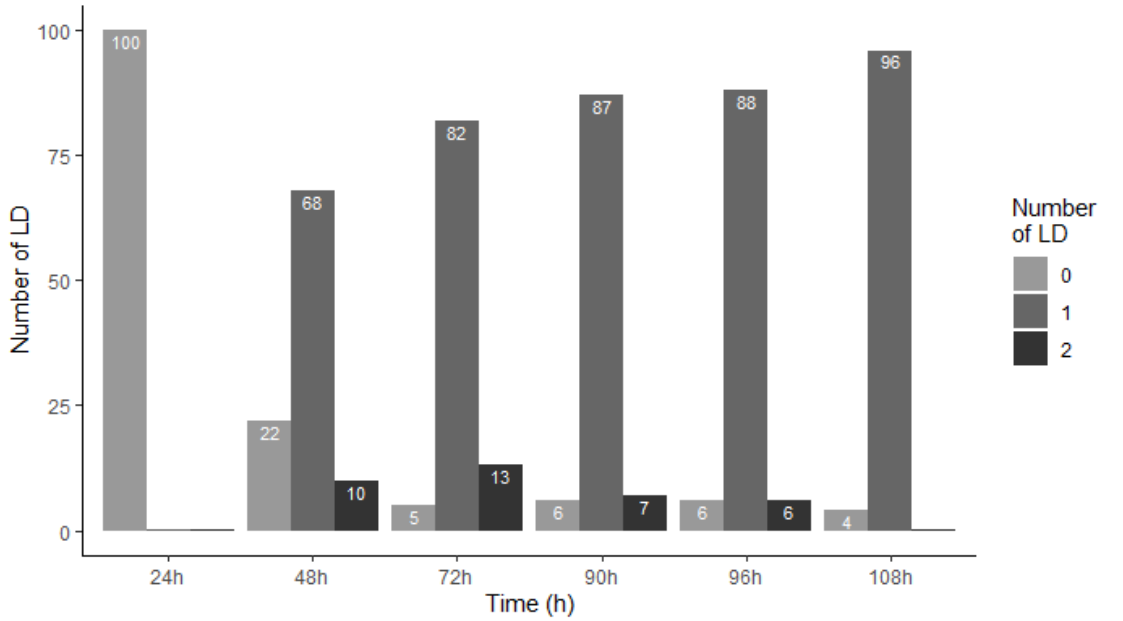

Figure 18. Count of the total of yeast cells (y-axis) with a specific number of LD per cell (grayscale) in different hours of growth (x-axis).

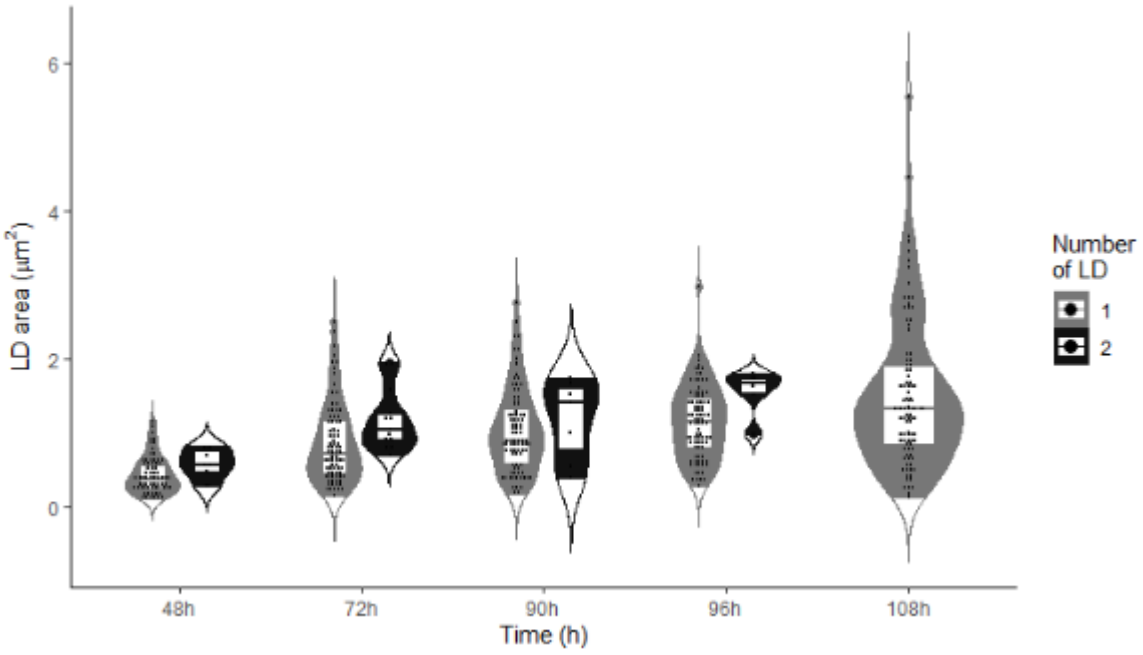

Figure 19. Analysis of the LDs area (y-axis) for a different number of lipid droplet finds per cell (grayscale) of *M. globosa* in different hours of growth (x-axis).

One possible explanation to the variations in size and number of LD observed could be the emerging of similar size LD from the ER and their subsequent increase in size by the incorporation of additional neutral lipids in response to the lipid sources available in the medium. This addition can be

promoted via the coalescence of LDs or the interaction between ER and these organelles.[123] In other yeasts, the donation of acyl groups from acyl-CoA and the accumulation of TAG and SE in LDs has been described at the stationary phase.[120,125,126] This process is mediated with the DGA1-encoded acyltransferase, which has been reported in *M. globosa.*[18]

When normalizing the data of the area of yeast, it was clear that LDs were growing in proportion to the size of the cell. The percentage of area occupied by the LD varied from a range of 2 to 15% in the exponential growth phase to a range of 5 to 50% in the late stationary phase (**Figure 20**). It was observed that the average area of LDs increases linearly over time, which can be related to Ostwald ripening phenomenon (**Figure 21**). In this process, the fusion of organelles, such as LD, occurs due to its micellar nature. The direction of this process depends on the difference in pressures of the two LDs, which cause that neutral lipids travel from a smaller LDs to a bigger one. This process causes one LDs to shrink while the other grows, as was observed for *M. globosa*.[44] This previous observation was evidenced in yeast cell with two LD, where one was bigger than the other.

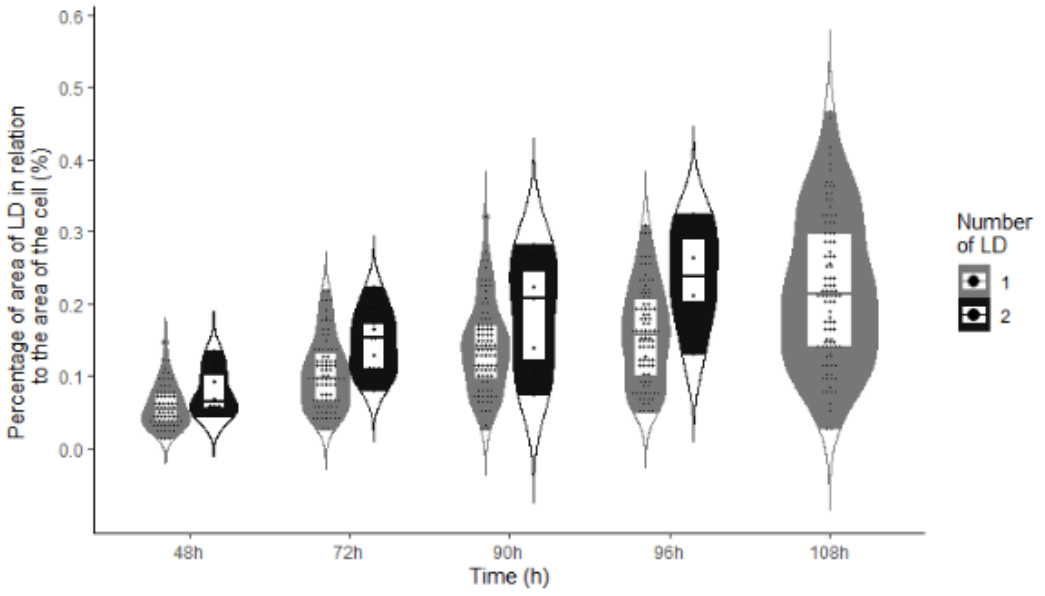

Figure 20. Analysis of the percentage of LD area about the area of the cell (y-axis) for the different number of lipid droplets per cell (grayscale) of *M. globosa* in different hours of growth (x-axis).

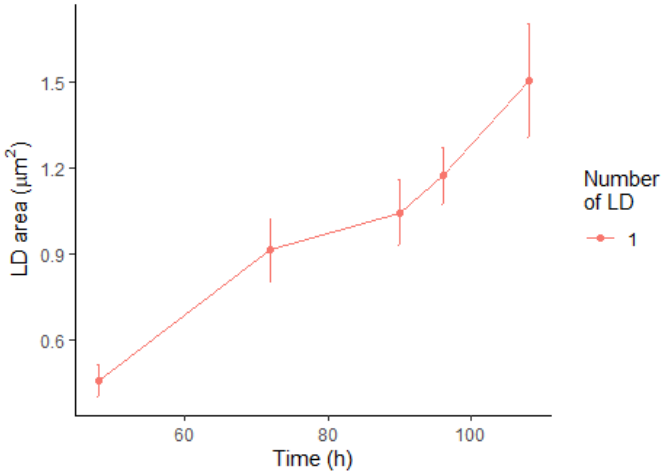

Figure 21. Mean area of LDs of *M. globosa*. Each error bar represents the interval of confidence for each time point.

The morphological analysis of LDs over time, no differences between the growth phases were observed using the circularity of LDs as a morphological parameter (**Figure 22**). In general, data showed a high variation in circularity, and results ranged from 0.4 up to 1.0. However, circularity trends were close to 1 for all the studied hours, confirming that these organelles are mostly round as expected.[44,47] For LDs with lower circularity value, a possible explanation relies on the coalescence process described above, where probably images were acquired while this process was occurring. Is important to note that "ripening of lipid droplets" is a slow process, taking several minutes to complete, giving sufficient time for images to be adcquired.[44]

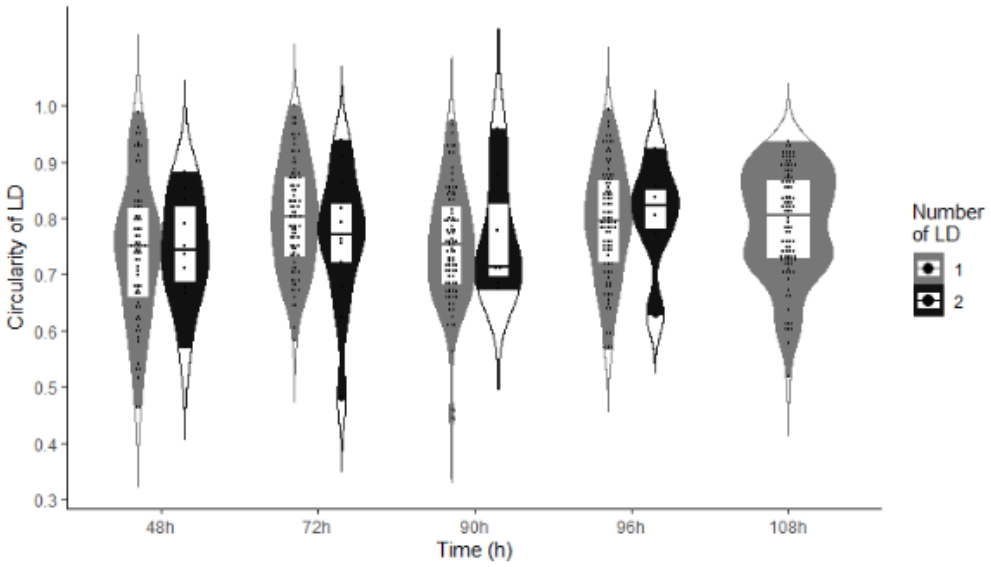

Figure 22. The circularity of Lipid droplets of *M. globosa* (y-axis) for the different number of lipid droplets find per cell (grayscale) of *M. globosa* in different hours of growth (x-axis).

4. Determination of the consumed and secreted lipids in *M. globosa.*

Lipids are usually classified into two categories, neutral or non-polar lipids (such as TAGs, DAGs, and ST) and more polar lipids (such as free FAs, GPLs, and SLs). Neutral lipids are easily dissolved in non-polar organic solvents, but polar lipids, especially phospholipids, only dissolve in relatively medium to strong polar solvents. In order to extract both types of lipids, it is necessary to use a solvent mixture sufficiently polar to dissolve the polar lipids but sufficiently non-polar to dissolve the neutral lipids. In this case, lipid extraction was performed by a modified Bligh and Dyer method.[61,89,90] This procedure starts with the dilution of the sample in a ternary mixture of water, MeOH, and chloroform 1:1:2, followed by vortex and ultrasonication procedure. MeOH is added to the extraction solution to promote the migration of polar lipids into the organic-rich phase. However, the amount of MeOH used must be carefully controlled because as more volume is added the solubility of neutral lipids in the organic-rich phase decreases drastically.[127]

The working principle of the extraction method relies on the Nerns't distribution law, also known as the distribution coefficient, which states that at a constant temperature, the ratio of concentrations at the equilibrium of a solubilized compound in a biphasic system is constant.[128] This means that by carefully selecting immiscible solvents for the extraction, it is possible to favor the migration of the desired analytes to one phase and the undesired compounds into the other phase. In this experiment, water was acidified with citric acid in order to protonate the carboxylate heads of the lipids, thus decreasing their water solubility and favoring their migration to the organic-rich phase.

Because this is an equilibrium-dependent method, a complete homogenization of the system must be performed to guarantee a good extraction performance.[128] The use of vortex and sonication serves this purpose. The vortex step enhances the migration of lipids to the organic-rich phase by increasing the rate of mass transports and decreasing the diffusion path length. The function of sonication is to destroy the aggregates formed during the extraction process, hindering their migration to the organic-rich phase. [128,129] A clear example of this phenomenon is the formation of micelles by phospholipids when they are in contact with water. Once formed, the polar phosphate and glycerol heads point toward the external part of the micelle, while the non-polar tails point inwards. These assemblies will not migrate to the organic-rich phase because the only part of the micelle that interacts with its surroundings is the polar one. Since these aggregates are thermodynamically stable, it is necessary to use a strong perturbation force to disassemble them, being, in this case, the implosion of the cavitation bubbles formed during the sonication process.[130]

To purify and preconcentrate the obtained lipids, a strong anion exchange solid phase extraction (SAX-SPE) was performed. Considering the complexity and lipid abundance of mDixon, SPE was a necessary process to concentrate non-polar lipids. Solid-phase extraction (SPE) is a separation principle using selective adsorption and selective elution. The cartridges used in this extraction are quaternary ammonium salts bonded to a silica matrix.[131] lipid crude was fixed to the stationary phase by a strong electrostatic interaction between the positively charged quaternary ammonium cations and the negatively charged functional groups in the lipids such as carboxylates and phosphate heads. The liquid/liquid extraction media was acidified to enhance separation, the solvents of the organic phase were evaporated, and the analytes were reconstituted in acetonitrile basified with ammonium hydroxide, to assured that lipids were in their anionic form. Once the sample was placed into the SAX SPE, the cartridge was washed with the solution of water/acetone to elute the most polar analytes and then washed with acetone to eliminate water traces. Finally, the elution of the cartage was performed with acidifying acetone to protonate the lipids and elute them from the stationary phase.[61,89,90]

A total of 463 molecular features were identified in the present study. Using these molecular features as lipid profiles, reduction of dimensionality via OPLS-DA was performed to determine the relevant compounds throughout the three treated groups. 146 molecular features were determined are represented by five orthogonal component analysis (**Supplementary figure 1**). Fresh mDixon displays the higher diversity and concentration of lipids compared to the groups of 72 hours and 90 hours post-culture. Between the last two groups, higher lipid profiles were observed at 72 hours, which is congruent with *Malassezia* lipid dependent metabolism.[2] However, there are some zones of the heatmap in which there is an intensity increase in 72 hours and 90 hours, indicating that *Malassezia* is also secreting some lipids. An abnormal secretion-consumption pattern was observed, in which some molecules were secreted at 72 hours and then consumed at 90 hours. This pattern was associated with the reduction of available metabolites through time. This pattern displays the highest variability among replicates, so molecules secreted might be related to the intrinsic biological differences among groups. Different replicates of the same sample groups, except for the replicate III of 72h, samples displayed similar patterns.

Based on a two-dimensional PCA analysis, there was a clear differentiation among groups. (**Figure 23**). Additionally, reproducibility in QC assures the good performance of the analytical platform. The variability of molecular features in the supernatant at 72 h and 90 h groups were higher than the

one in mDixon. This can be associated with an intrinsic biological variation of the samples, where slightest aleatory changes in growth conditions can affect the lipid expression.[132] When observing the PCA analysis excluding the mDixon control, there was a differentiation between treatment groups (**Figure 24**). Additionally, the replicate III in 72 hours is significantly different from two the other replicates for the same time of culture. This could be related to abnormal growth in this sample, where some lipids where more secreted than in other samples (**Supplementary figure 1**).

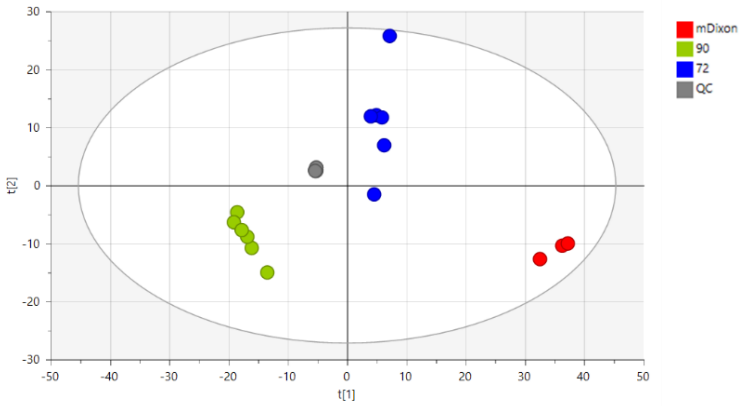

Figure 23. PCA-X score plots for samples, mDixon control and QC samples. Red: mDixon control, Green: 90 h sample, Blue: 72 h sample and Gray: QC samples. R^2 = 0.987 Q^2 = 0.944. Ellipse Hotelling´s T2 at α 0.05 is displayed.

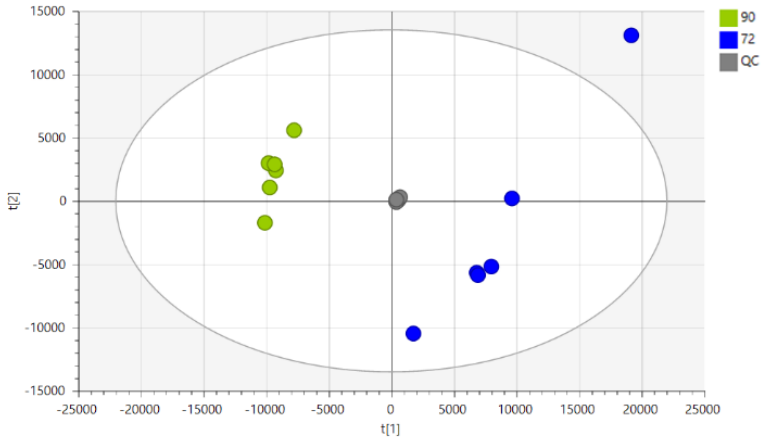

Figure 24. PCA-X score plots for treatment samples and QC samples. Green: 90 h sample, Blue: 72 h sample and Gray: QC samples. R2 = 0.987 Q2 = 0.944. Ellipse Hotelling´s T2 at α 0.05 is displayed.

Identification of molecular features based on the exact precursor mass and retention time was performed. 76 lipids of 11 different families were identified (**Figure 25**). Further analysis including the product ionization spectra are needed to confirm the identity of all these lipids. The majority of

families identified are neutral but polarizable lipids, which are more efficiently analyzed in positive detection mode.[133,134] Lipid classes in this category include PC, lysoPC, PE, SM, DAG, TAG, Sterols, etc.[135] Also cardiolipins (CL), usually detected in negative ionization mode, can be identified in positive ionization mode.[136,137]

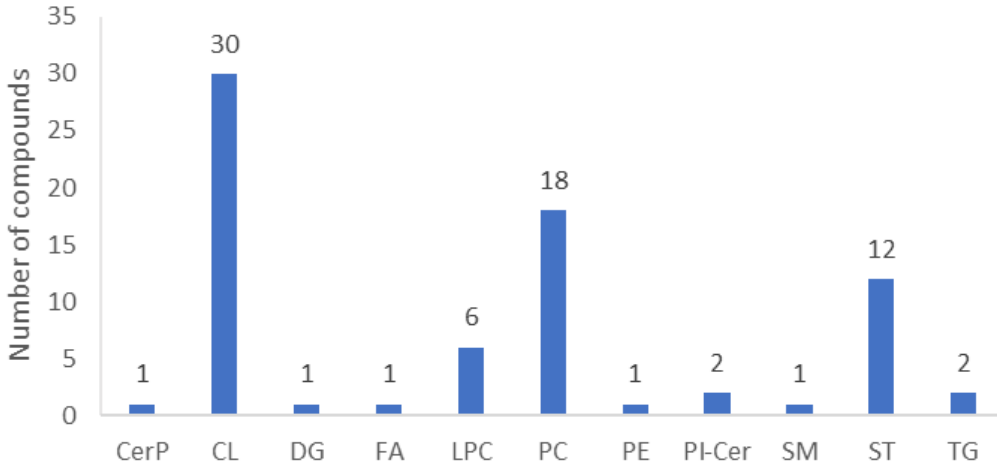

Figure 25. The number of compounds identified for different lipid families. CerP: Ceramide phosphate. CL: Cardiolipins, DG: diglyceryl. FA: Fatty acid. GlcCer: Glycosylated ceramides- LPC: Lysophosphatidylcholine. LPE: Lysophosphatidylethanolamine. PC: Phosphatidylcholine. PE: phosphatidylethanolamine. PI-Cer: Ceramide phosphoinositol. SM: Sphingomyelins. ST: Sterols. TG: Triglycerides.

Most of the identified families in this study were described previously *in M. globosa*.[18] The ceramide phosphoinositol, which was not described in the study mentioned above, has been previously described in *Saccharomyces cerevisiae*.[138] The three categories observed **(Figure 25 and supplementary figure 1)** were also identified by Celis Ramírez, A.M et al.[18] Based on the results obtained, there was both a decrease and a increase on relative intensities for different molecular features in supernatant, implying that they could be a consumption and secretion of the lipids by the yeast. There was a higher number of molecular features for which the reduction in intensity was significant, suggesting that the percentage of possible lipid profiles that were consumed has higher. These results go in concordance with the lipid dependent metabolism of *M. globosa.* This medium is composed of a wide variety of lipids, including oleic acid, tween 40, glycerol, and the lipids present in ox bile, maltose, and peptone. Ox bile contains all of the constituents characteristic found in bile, including cholesterol, bile acids, GPLs, GLs, and TAGs.[139,140] Peptone is a protein hydrolysate that contains a small percentage of lipids, while malt extract, prepared from sprouted grains, might contain lipids as well.[141] For the discriminatory variables detected and identified in this study, the

majority are a common component of mammal bile include cholic acids and different phospholipids.[142] Some of the TAGs and acylglycerols identified are generated by a biochemical synthesis in the bile and are present in mDixon.[141,143]

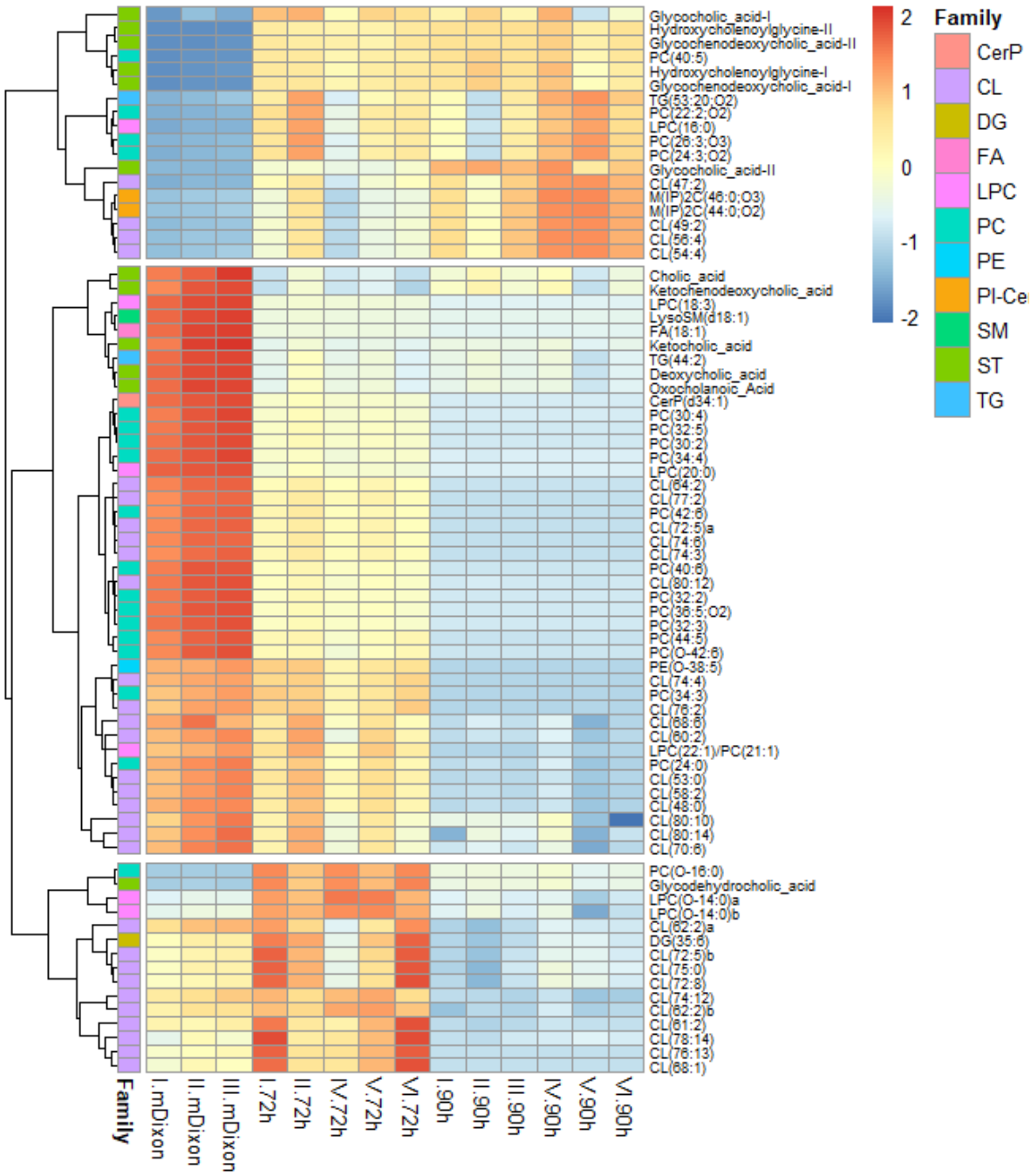

Figure 26. Heat map of identified molecular features for differentiation of the fresh mDixon and supernatant of 72h and 90h of *M. globosa* growth. The heat map denotes the higher (red) to lower (blue) relative intensity for each molecular

feature. Replicate three in 72 hours was removed for a better picturing of patterns. Hierarchical divisions based on clustering are displayed, showing the different intake-secretion patterns

Based on the tentative identification done, cholesterol was detected in all groups (controls and treatment), with a small percentage in treatment groups. There were significant differences among their relative intensities (Data not shown). A higher concentration of this molecule was detected in yeast controls, which is in concordance with the biosynthesis of ST reported and the presence of this molecule for this specie.[18] A higher percentage of CL and PC were detected in the present study in M. *globosa*.[18] Also, some of the molecules observed in supernatant could be produced by the lipases, phospholipases, sphingomyelinases, and lipoxygenases responsible of degrading sebum.[2,5,7,12]

Interestingly, acidic lipids, specifically CL, seem to have a dynamic role in *M. globosa* energetic adaptation. It was observed that a considerable number of the consumed lipids were CL, which can be related to its fundamental role in the translation of electron transport chain components and stabilization of mitochondrial DNA in yeast.[144,145] These lipids are essential in the stress-response of yeasts, which can be caused by the decrease of available resources in mDixon media through time.[144,146] Additionally, CL can be used as metabolic blocks, specifically in the synthesis of phosphatidic acid through the phospholipase D.[147]

The secretion of some CL was also observed in 72 h and 90 h groups. Considering that CL synthase is present in *M. globosa* as well as its precursors, synthesis *de novo* is possible in this cell. Specifically, cytidine diphosphate DAGs is a crucial intermediate in the synthesis of CL.[54] Enzymes associated with this metabolic pathway have been found previously in *M. globosa.*[18] This can generate an excess of these molecules in the cell, which could affect cell membrane structure stability and shape.[148] To maintain optimal concentrations of CL, possible secretion might be occurring in response to the growth conditions.[149] The secretion-consumption pattern could represent a recycling cycle where the excess of CL secreted and can be later used by new budding yeasts when resources are limited in the growth medium.

Also, some bile acids were consumed by the yeast. Bile acids have been related to both a beneficial and a prejudicial effect in yeasts. On the one hand, lithocholic acid has been linked to alteration on the age-related process in *S. cerevisiae*, increasing its lifespan through the variation in mitochondrial membrane lipidome. Therefore, the consumption of these external acids might help in cell maintenance.[150,151] However, the same acid has been related to fungistatic activities in other yeast

such as *C. albicans.*[152,153] This suggests that the effect of bile acids varies among different yeast species. In the case of *M. globosa*, the consumption of cholic acids and some derivates was observed. In contrast, the excretion of glycocholic acids and its derivates occur in both 72h and 90h groups, suggesting that nitrogenated bile acids might have a negative effect on *Malassezia* growth; therefore, they are secreted to avoid toxicity.

Different kinds of glycerophospholipids were found in the consumed analysis. These molecules are essential in yeast growth as PE is the major membrane component, while PCs have been related to mitochondrial functions.[16,154] PC also has highly dynamic role in LD formation. [44,155] The PC concentration could highly influence the process of coalescence in LDs observed for *M. globosa*, and its effectiveness could depend on the curvature of the monolayer of LD, which is defined primarily by the lipids that compose that monolayer. When two LDs approach, the fusion process can be either frustrated or effective depending on the spontaneous curvature on the membrane. When the curvature of the membrane is positive, the operation is frustrated due to high tension of membranes, but when it is negative, the pore is stabilized and open further, resulting in LD fusion.[44] Neutral nature of PC and its conformation provides excellent coverage of the surface area and lowers surface tension, making of this molecule important in LD stability and increasing the probability of coalescence mechanism to occur.[44] It was also observed that oleic acid was consumed but not secreted by the cell, however, low concentration of FA has been described in *M. globosa* lipidome.[18] Storage of these molecules in LD probably is occurring to avoid toxicity within the cell.[12] Additional, as *M. globosa* lack of the ability to produce unsaturated FAs such as oleic acid, this lipid is probably consumed by this yeast to support their growth, acting as building block for complex lipids.[2,18]

Oxidized phospholipids, especially PC, were detected as secretory products within the cell. It is speculated that a high percentage of oxidized products in biological samples are likely to form by non-enzymatic reactions.[156] However, enzymes such as lipoxygenases, previously described in *M. globosa,* can be responsible for the appearance of these molecules.[111,156] Accumulation of the oxidized lipids is associated with danger signals; as they can generate oxidative stress and cell death, therefore its secretion may help in the regulation of their harmful effect.[157] Interestingly, secretion of these molecules might be related to *Malassezia* pathogenic role, as these molecules influence the decisive steps of the adaptive immune response, regulation of dendritic cell maturation, and function.[157] The concentration of oxidized lipids increased in time, as the availability of nutrients in mDixon decreased, implying that changes in metabolites inside the cell can trigger the production

of these types of lipids, and therefore induce a pathogenic *Malassezia* effect. Further studies should be carried out in order to confirm this hypothesis.

Finally, some phosphosphingolipids, specifically ceramide phosphoinositols (PI-Cer), were observed in the analysis. These molecules had been described previously as common complex phosphosphingolipids in *Saccharomyces cerevisiae* but not in M*alassezia.*[138] Ceramide phosphoinositol transferase and phosphatidylinositol synthase, enzymes important in the synthesis of PI-Cer, were found by Celis Ramírez, AM et al.[18,158] These molecules regulate the virulence in *Cryptococcus neoformans* by inducing the transcription of virulence factors, and promoting cell wall stability and melanine production.[158,159] Based on this information, the secretion of PI-Cer might influence the pathogenic facet of *M. globosa.*

IX. Conclusions and perspectives

A protocol for the extraction of LDs was developed for *M. globosa*, however further purification methods are still needed to clean up the organelles extracted. Also, a protocol for confocal microscopy fluorescence double staining of LDs in *M. globosa* was standardized using three different fluorophores: NR, BODIPY 493/503, and LipidTOX deep red neutral. The dynamics of LDs formation was described as qualitative and quantitively. It was found that LDs starts forming in *M. globosa* after 48 hours post-culture during the exponential growth phase. Future studies in LD biogenesis are necessary to understand this biological process. Analysis of LDs showed that there was an increase in the variation of LDs area in *M. globosa,* and the number of LDs decrease as the yeast entered the stationary phase. Additionally, a linear relationship was observed between the LDs area and time. Based on these observations, a coalescence pattern was proposed.

Also, lipid profiles from mDixon, in early and late stationary phases were differentiated via principal component analysis (PCA). The analysis showed 77 lipids from 11 different families; those lipids were assigned based on their molecular weight. Further analysis are needed to confirm the identity of each individual lipid. In general, there is a higher percentage of lipids consumed by *M. globosa* in comparison to the secreted lipids. From the families detected, CL and PC seem to have a dynamic role in *M. globosa* adaptation. Additionally, oxidized lipids such as GPLs and PI-Cer were identified, and it is hypothesized that these might play a role in the pathogenesis of this yeast. Finally, to acquire a complete profile of the lipids present in the processes of consumption and secretion in *M. globosa*, a study in negative ionization mode should be carried out, specifically to identify lipids like phosphatidylserine, phosphatidic acids and FAHFAs that were not detected in this analysis.

X. References

(1) Guého-Kellermann, E.; Boekhout, T.; Begerow, D. Biodiversity, Phylogeny and Ultrastructure. In *Malassezia and the Skin*; Springer Berlin Heidelberg: Berlin, Heidelberg, 2010; pp 17–63. https://doi.org/10.1007/978-3-642-03616-3_2.

(2) Triana, S.; de Cock, H.; Ohm, R. A.; Danies, G.; Wösten, H. A. B.; Restrepo, S.; González Barrios, A. F.; Celis, A. Lipid Metabolic Versatility in *Malassezia* spp. Yeasts Studied through Metabolic Modeling. *Front. Microbiol.* **2017**, *8*. https://doi.org/10.3389/fmicb.2017.01772.

(3) Grice, E. A.; Dawson Jr, T. L. Host – Microbe Interactions : *Malassezia* and Human Skin. *Curr. Opin. Microbiol.* **2017**, *40*, 81–87. https://doi.org/10.1016/j.mib.2017.10.024.

(4) Celis, A.; Wösten, H.; Triana, S.; Restrepo, S.; de Cock, H. *Malassezia* spp. beyond the Mycobiota. *SM Dermatology J.* **2017**, *3* (3), 1019. https://doi.org/10.36876/smdj.1019.

(5) Xu, J.; Saunders, C. W.; Hu, P.; Grant, R. A.; Boekhout, T.; Kuramae, E. E.; Kronstad, J. W.; DeAngelis, Y. M.; Reeder, N. L.; Johnstone, K. R.; Leland, M.; Fieno, A. M.; Begley, W. M.; Sun, Y.; Lacey, M. P.; Chaudhary, T.; Keough, T.; Chu, L.; Sears, R.; Yuan, B.; Dawson, T. L. Dandruff-Associated *Malassezia* Genomes Reveal Convergent and Divergent Virulence Traits Shared with Plant and Human Fungal Pathogens. *Proc. Natl. Acad. Sci.* **2007**, *104* (47), 18730–18735. https://doi.org/10.1073/pnas.0706756104.

(6) Velegraki, A.; Cafarchia, C.; Gaitanis, G.; Iatta, R.; Boekhout, T. *Malassezia* Infections in Humans and Animals: Pathophysiology, Detection, and Treatment. *PLoS Pathog.* **2015**, *11* (1), e1004523. https://doi.org/10.1371/journal.ppat.1004523.

(7) Boekhout, T.; Guého, E.; Mayser, P.; Velegraki, A. *Malassezia and the Skin: Science and Clinical Practice*; 2010. https://doi.org/10.1007/978-3-642-03616-3.

(8) Caban, F. J. *Malassezia* Yeasts : How Many Species Infect Humans and Animals ? *PLoS Pathog.* **2014**, *10* (2), e1003892. https://doi.org/10.1371/journal.ppat.1003892.

(9) Wu, G.; Zhao, H.; Li, C.; Rajapakse, M. P.; Wong, W. C.; Xu, J.; Saunders, C. W.; Reeder, N. L.; Reilman, R. A.; Scheynius, A.; Sun, S.; Billmyre, B. R.; Li, W.; Averette, A. F.; Mieczkowski, P.; Heitman, J.; Theelen, B.; Schröder, M. S.; De Sessions, P. F.; Butler, G.; Maurer-Stroh, S.; Boekhout, T.; Nagarajan, N.; Dawson, T. L. Genus-Wide Comparative Genomics of *Malassezia*

Delineates Its Phylogeny, Physiology, and Niche Adaptation on Human Skin. *PLOS Genet.* **2015**, *11* (11), e1005614. https://doi.org/10.1371/journal.pgen.1005614.

(10) Lorch, J. M.; Palmer, J. M.; Vanderwolf, K. J.; Schmidt, K. Z.; Verant, M. L.; Weller, T. J.; Blehert, D. S. *Malassezia vespertilionis* Sp. Nov.: A New Cold-Tolerant Species of Yeast Isolated from Bats. *Persoonia - Mol. Phylogeny Evol. Fungi* **2018**, *41* (1), 56–70. https://doi.org/10.3767/persoonia.2018.41.04.

(11) Raugi, G.; Nguyen, T. U. Superficial Dermatophyte Infections of the Skin. In *Netter's Infectious Diseases*; Elsevier, 2012; pp 102–109. https://doi.org/10.1016/B978-1-4377-0126-5.00022-7.

(12) Celis, A. M. Unraveling Lipid Metabolism in Lipid-Dependent Pathogenic *Malassezia* Yeasts, Utrecht University, 2017.

(13) Olzmann, J. A.; Carvalho, P. Dynamics and Functions of Lipid Droplets. *Nat. Rev. Mol. Cell Biol.* **2019**, *20*, 137–155. https://doi.org/10.1038/s41580-018-0085-z.

(14) Rambold, A. S.; Cohen, S.; Lippincott-Schwartz, J. Fatty Acid Trafficking in Starved Cells: Regulation by Lipid Droplet Lipolysis, Autophagy, and Mitochondrial Fusion Dynamics. *Dev. Cell* **2015**, *32* (6), 678–692. https://doi.org/10.1016/j.devcel.2015.01.029.

(15) Klug, L.; Daum, G. Yeast Lipid Metabolism at a Glance. *FEMS Yeast Res.* **2014**, *14* (3), 369–388. https://doi.org/10.1111/1567-1364.12141.

(16) Horvath, S. E.; Wagner, A.; Steyrer, E.; Daum, G. Metabolic Link between Phosphatidylethanolamine and Triacylglycerol Metabolism in the Yeast Saccharomyces Cerevisiae. *Biochim. Biophys. Acta - Mol. Cell Biol. Lipids* **2011**, *1811* (12), 1030–1037. https://doi.org/10.1016/j.bbalip.2011.08.007.

(17) Shea, J. M.; Henry, J. L.; Del Poeta, M. Lipid Metabolism in *Cryptococcus neoformans*. *FEMS Yeast Res.* **2006**, *6* (4), 469–479. https://doi.org/10.1111/j.1567-1364.2006.00080.x.

(18) Celis Ramírez, A. M.; Amézquita, A.; Cardona, J.; Matiz Cerón, L. F.; Andrade-Martínez, J. S.; Triana, S.; Mantilla, M. J.; Restrepo, S.; González Barrios, A. F.; Cock, H. *Analysis of Malassezia Lipidome Disclosed Differences among the Species and Reveals Presence of Unusual Yeast Lipids*; 2020.

(19) Simpson, C. L.; Patel, D. M.; Green, K. J. Deconstructing the Skin: Cytoarchitectural Determinants of Epidermal Morphogenesis. *Nat. Rev. Mol. Cell Biol.* **2011**, *12* (9), 565–580. https://doi.org/10.1038/nrm3175.

(20) Kaplan, D. H.; Igyártó, B. Z.; Gaspari, A. A. Early Immune Events in the Induction of Allergic Contact Dermatitis. *Nat. Rev. Immunol.* **2012**, *12* (2), 114–124. https://doi.org/10.1038/nri3150.

(21) Murphy, K. *Janeway's Immunobiology*; Garland Science: 9th edition. | New York, NY : Garland Science/Taylor & Francis, 2016. https://doi.org/10.1201/9781315533247.

(22) Findley, K.; Oh, J.; Yang, J.; Conlan, S.; Deming, C.; Meyer, J. A.; Schoenfeld, D.; Nomicos, E.; Park, M.; Kong, H. H.; Segre, J. A. Topographic Diversity of Fungal and Bacterial Communities in Human Skin. *Nature* **2013**, *498* (7454), 367–370. https://doi.org/10.1038/nature12171.

(23) Roth, R. R.; James, W. D. Microbial Ecology of the Skin. *Annu. Rev. Microbiol.* **1988**, *42* (1), 441–464. https://doi.org/10.1146/annurev.mi.42.100188.002301.

(24) White, T. C.; Findley, K.; Dawson, T. L.; Scheynius, A.; Boekhout, T.; Cuomo, C. A.; Xu, J.; Saunders, C. W. Fungi on the Skin: Dermatophytes and *Malassezia*. *Cold Spring Harb. Perspect. Med.* **2014**, *4* (8), a019802–a019802. https://doi.org/10.1101/cshperspect.a019802.

(25) Harada, K.; Saito, M.; Sugita, T.; Tsuboi, R. *Malassezia* species and Their Associated Skin Diseases. *J. Dermatol.* **2015**, *42* (3), 250–257. https://doi.org/10.1111/1346-8138.12700.

(26) Wilson, M. *The Human Microbiota in Health and Disease*; Garland Science: Boca Raton, FL : CRC Press, Taylor & Francis Group, 2019., 2018. https://doi.org/10.1201/9781351068369.

(27) Saunders, C. W.; Scheynius, A.; Heitman, J. *Malassezia* Fungi Are Specialized to Live on Skin and Associated with Dandruff, Eczema, and Other Skin Diseases. *PLoS Pathog.* **2012**, *8* (6), e1002701. https://doi.org/10.1371/journal.ppat.1002701.

(28) Dokos, C.; Pana, Z.-D.; Tragiannidis, A. *Malassezia* species: A Rare Cause of Invasive Fungal Infections in Immunocompromised Patients. *Curr. Fungal Infect. Rep.* **2011**, *5* (1), 18–22. https://doi.org/10.1007/s12281-010-0037-3.

(29) DeAngelis, Y. M.; Saunders, C. W.; Johnstone, K. R.; Reeder, N. L.; Coleman, C. G.; Kaczvinsky,

J. R.; Gale, C.; Walter, R.; Mekel, M.; Lacey, M. P.; Keough, T. W.; Fieno, A.; Grant, R. A.; Begley, B.; Sun, Y.; Fuentes, G.; Scott Youngquist, R.; Xu, J.; Dawson, T. L. Isolation and Expression of a *Malassezia globosa* Lipase Gene, LIP1. *J. Invest. Dermatol.* **2007**, *127* (9), 2138–2146. https://doi.org/10.1038/sj.jid.5700844.

(30) Juntachai, W.; Oura, T.; Murayama, S. Y.; Kajiwara, S. The Lipolytic Enzymes Activities of *Malassezia* species. *Med. Mycol.* **2009**, *47* (5), 477–484. https://doi.org/10.1080/13693780802314825.

(31) Gupta, A. K.; Kohli, Y.; Summerbell, R. C. Molecular Differentiation of Seven *Malassezia* species. *J. Clin. Microbiol.* **2000**, *38* (5), 1869–1875.

(32) Gaitanis, G.; Magiatis, P.; Stathopoulou, K.; Bassukas, I. D.; Alexopoulos, E. C.; Velegraki, A.; Skaltsounis, A.-L. AhR Ligands, Malassezin, and Indolo[3,2-b]Carbazole Are Selectively Produced by *Malassezia furfur* Strains Isolated from Seborrheic Dermatitis. *J. Invest. Dermatol.* **2008**, *128* (7), 1620–1625. https://doi.org/10.1038/sj.jid.5701252.

(33) Cafarchia, C.; Otranto, D. Association between Phospholipase Production by *Malassezia pachydermatis* and Skin Lesions. *J. Clin. Microbiol.* **2004**, *42* (10), 4868–4869. https://doi.org/10.1128/JCM.42.10.4868-4869.2004.

(34) Cafarchia, C.; Gasser, R. B.; Latrofa, M. S.; Parisi, A.; Campbell, B. E.; Otranto, D. Genetic Variants of *Malassezia pachydermatis* from Canine Skin: Body Distribution and Phospholipase Activity. *FEMS Yeast Res.* **2008**, *8* (3), 451–459. https://doi.org/10.1111/j.1567-1364.2008.00358.x.

(35) Cafarchia, C.; Dell'aquila, M. E.; Traversa, D.; Albrizio, M.; Guaricci, A. C.; de Santis, T.; Otranto, D. Expression of the μ-Opioid Receptor on *Malassezia pachydermatis* and Its Effect in Modulating Phospholipase Production. *Med. Mycol.* **2010**, *48* (1), 73–78. https://doi.org/10.3109/13693780902718347.

(36) Aldana, J.; Romero-Otero, A.; Cala, M. P. Exploring the Lipidome: Current Lipid Extraction Techniques for Mass Spectrometry Analysis. *Metabolites* **2020**, *10* (6), 231. https://doi.org/10.3390/metabo10060231.

(37) Yang, K.; Han, X. Lipidomics: Techniques, Applications, and Outcomes Related to Biomedical Sciences. *Trends Biochem. Sci.* **2016**, *41* (11), 954–969.

https://doi.org/10.1016/j.tibs.2016.08.010.

(38) Fahy, E.; Cotter, D.; Sud, M.; Subramaniam, S. Lipid Classification, Structures and Tools. *Biochim. Biophys. Acta - Mol. Cell Biol. Lipids* **2011**, *1811* (11), 637–647. https://doi.org/10.1016/j.bbalip.2011.06.009.

(39) Fahy, E.; Subramaniam, S.; Brown, H. A.; Glass, C. K.; Merrill, A. H.; Murphy, R. C.; Raetz, C. R. H.; Russell, D. W.; Seyama, Y.; Shaw, W.; Shimizu, T.; Spener, F.; van Meer, G.; VanNieuwenhze, M. S.; White, S. H.; Witztum, J. L.; Dennis, E. A. A Comprehensive Classification System for Lipids. *J. Lipid Res.* **2005**, *46* (5), 839–862. https://doi.org/10.1194/jlr.E400004-JLR200.

(40) Postle, A. D. Lipidomics. *Curr. Opin. Clin. Nutr. Metab. Care* **2012**, 1. https://doi.org/10.1097/MCO.0b013e32834fb003.

(41) Wang, M.; Wang, C.; Han, R. H.; Han, X. Novel Advances in Shotgun Lipidomics for Biology and Medicine. *Prog. Lipid Res.* **2016**, *61*, 83–108. https://doi.org/10.1016/j.plipres.2015.12.002.

(42) Köfeler, H. C.; Fauland, A.; Rechberger, G. N.; Trötzmüller, M. Mass Spectrometry Based Lipidomics: An Overview of Technological Platforms. *Metabolites* **2012**, *2* (1), 19–38. https://doi.org/10.3390/metabo2010019.

(43) Radulovic, M.; Knittelfelder, O.; Cristobal-Sarramian, A.; Kolb, D.; Wolinski, H.; Kohlwein, S. D. The Emergence of Lipid Droplets in Yeast: Current Status and Experimental Approaches. *Curr. Genet.* **2013**, *59* (4), 231–242. https://doi.org/10.1007/s00294-013-0407-9.

(44) Thiam, A. R.; Farese Jr, R. V.; Walther, T. C. The Biophysics and Cell Biology of Lipid Droplets. *Nat. Rev. Mol. Cell Biol.* **2013**, *14* (12), 775–786. https://doi.org/10.1038/nrm3699.

(45) Xu, S.; Zhang, X.; Liu, P. Lipid Droplet Proteins and Metabolic Diseases. *Biochim. Biophys. Acta - Mol. Basis Dis.* **2018**, *1864* (5), 1968–1983. https://doi.org/10.1016/j.bbadis.2017.07.019.

(46) Martin, M. L. Role of the Regulation of Cell Lipid Composition and Membrane Structure in the Antitumor Effect of 2-Hydroxyoleic Acid, Universitat de les Illes Balears, 2011.

(47) Choudhary, V.; Golani, G.; Joshi, A. S.; Cottier, S.; Schneiter, R.; Prinz, W. A.; Kozlov, M. M. Architecture of Lipid Droplets in Endoplasmic Reticulum Is Determined by Phospholipid

Intrinsic Curvature. *Curr. Biol.* **2018**, *28* (6), 915-926.e9. https://doi.org/10.1016/j.cub.2018.02.020.

(48) Onal, G.; Kutlu, O.; Gozuacik, D.; Dokmeci Emre, S. Lipid Droplets in Health and Disease. *Lipids Health Dis.* **2017**, *16* (1), 128. https://doi.org/10.1186/s12944-017-0521-7.

(49) Wang, C.-W. Lipid Droplet Dynamics in Budding Yeast. *Cell. Mol. Life Sci.* **2015**, *72* (14), 2677–2695. https://doi.org/10.1007/s00018-015-1903-5.

(50) Xu, D.; Li, Y.; Wu, L.; Li, Y.; Zhao, D.; Yu, J.; Huang, T.; Ferguson, C.; Parton, R. G.; Yang, H.; Li, P. Rab18 Promotes Lipid Droplet (LD) Growth by Tethering the ER to LDs through SNARE and NRZ Interactions. *J. Cell Biol.* **2018**, *217* (3), 975–995. https://doi.org/10.1083/jcb.201704184.

(51) Pol, A.; Gross, S. P.; Parton, R. G. Biogenesis of the Multifunctional Lipid Droplet: Lipids, Proteins, and Sites. *J. Cell Biol.* **2014**, *204* (5), 635–646. https://doi.org/10.1083/jcb.201311051.

(52) Madeira, J. B.; Masuda, C. A.; Maya-Monteiro, C. M.; Matos, G. S.; Montero-Lomelí, M.; Bozaquel-Morais, B. L. TORC1 Inhibition Induces Lipid Droplet Replenishment in Yeast. *Mol. Cell. Biol.* **2015**, *35* (4), 737–746. https://doi.org/10.1128/MCB.01314-14.

(53) Gibellini, F.; Smith, T. K. The Kennedy Pathway-De Novo Synthesis of Phosphatidylethanolamine and Phosphatidylcholine. *IUBMB Life* **2010**, n/a-n/a. https://doi.org/10.1002/iub.337.

(54) Blunsom, N. J.; Cockcroft, S. CDP-Diacylglycerol Synthases (CDS): Gateway to Phosphatidylinositol and Cardiolipin Synthesis. *Front. Cell Dev. Biol.* **2020**, *8*. https://doi.org/10.3389/fcell.2020.00063.

(55) Alouf., J. E.; Popoff, M. R. *The Comprehensive Sourcebook of Bacterial Protein Toxins*; Elsevier, 2006. https://doi.org/10.1016/B978-0-12-088445-2.X5000-8.

(56) Tirinato, L.; Pagliari, F.; Limongi, T.; Marini, M.; Falqui, A.; Seco, J.; Candeloro, P.; Liberale, C.; Di Fabrizio, E. An Overview of Lipid Droplets in Cancer and Cancer Stem Cells. *Stem Cells Int.* **2017**, *2017*, 1–17. https://doi.org/10.1155/2017/1656053.

(57) Sui, X.; Arlt, H.; Brock, K. P.; Lai, Z. W.; Dimaio, F.; Marks, D. S.; Liao, M.; Jr, R. V. F. Cryo – Electron Microscopy Structure of the Lipid Droplet – Formation Protein Seipin. *J. Cell Biol.*

2018, *217* (12), 4080–4091. https://doi.org/10.1083/jcb.201809067.

(58) Miyanari, Y.; Atsuzawa, K.; Usuda, N.; Watashi, K.; Hishiki, T.; Zayas, M.; Bartenschlager, R.; Wakita, T.; Hijikata, M.; Shimotohno, K. The Lipid Droplet Is an Important Organelle for Hepatitis C Virus Production. *Nat. Cell Biol.* **2007**, *9* (9), 1089–1097. https://doi.org/10.1038/ncb1631.

(59) Ferguson, D.; Zhang, J.; Davis, M. A.; Helsley, R. N.; Vedin, L. L.; Lee, R. G.; Crooke, R. M.; Graham, M. J.; Allende, D. S.; Parini, P.; Brown, J. M. The Lipid Droplet-Associated Protein Perilipin 3 Facilitates Hepatitis C Virus-Driven Hepatic Steatosis. *J. Lipid Res.* **2017**, *58* (2), 420–432. https://doi.org/10.1194/jlr.M073734.

(60) Herker, E.; Ott, M. Emerging Role of Lipid Droplets in Host / Pathogen Interactions. *J. Biol. chemestry* **2012**, *287* (4), 2280–2287. https://doi.org/10.1074/jbc.R111.300202.

(61) Zhu, Q.-F.; Yan, J.-W.; Gao, Y.; Zhang, J.-W.; Yuan, B.-F.; Feng, Y.-Q. Highly Sensitive Determination of Fatty Acid Esters of Hydroxyl Fatty Acids by Liquid Chromatography-Mass Spectrometry. *J. Chromatogr. B* **2017**, *1061–1062*, 34–40. https://doi.org/10.1016/j.jchromb.2017.06.045.

(62) Armstrong, R. M.; Carter, D. C.; Atkinson, S. N.; Terhune, S. S.; Zahrt, T. C. Association of *Mycobacterium* Proteins with Lipid Droplets. *J. Bacteriol.* **2018**, *200* (16), e00240-18. https://doi.org/10.1128/JB.00240-18.

(63) Zhu, Z.; Ding, Y.; Gong, Z.; Yang, L.; Zhang, S.; Zhang, C.; Lin, X.; Shen, H.; Zou, H.; Xie, Z.; Yang, F.; Zhao, X.; Liu, P.; Zhao, Z. K. Dynamics of the Lipid Droplet Proteome of the Oleaginous Yeast *Rhodosporidium toruloides*. *Eukaryot. Cell* **2015**, *14* (3), 252–264. https://doi.org/10.1128/EC.00141-14.

(64) Listenberger, L. L.; Brown, D. A. Fluorescent Detection of Lipid Droplets and Associated Proteins. *Curr. Protoc. Cell Biol.* **2007**, *35* (1), 24.2.1-24.2.11. https://doi.org/10.1002/0471143030.cb2402s35.

(65) Fam, T.; Klymchenko, A.; Collot, M. Recent Advances in Fluorescent Probes for Lipid Droplets. *Materials (Basel).* **2018**, *11* (9), 1768. https://doi.org/10.3390/ma11091768.

(66) Narayan, R. J. *Monitoring and Evaluation of Biomaterials and Their Performance In Vivo*; Elsevier, 2017. https://doi.org/10.1016/C2014-0-04050-6.

(67) Klapper, M.; Ehmke, M.; Palgunow, D.; Böhme, M.; Matthäus, C.; Bergner, G.; Dietzek, B.; Popp, J.; Döring, F. Fluorescence-Based Fixative and Vital Staining of Lipid Droplets in *Caenorhabditis elegans* Reveal Fat Stores Using Microscopy and Flow Cytometry Approaches. *J. Lipid Res.* **2011**, *52* (6), 1281–1293. https://doi.org/10.1194/jlr.D011940.

(68) Gao, Q.; Binns, D. D.; Kinch, L. N.; Grishin, N. V; Ortiz, N.; Chen, X.; Goodman, J. M. Pet10p Is a Yeast Perilipin That Stabilizes Lipid Droplets and Promotes Their Assembly. *J. Cell Biol.* **2017**, 1–19.

(69) Ding, Y.; Zhang, S.; Yang, L.; Na, H.; Zhang, P.; Zhang, H.; Wang, Y.; Chen, Y.; Yu, J.; Huo, C.; Xu, S.; Garaiova, M.; Cong, Y.; Liu, P. Isolating Lipid Droplets from Multiple Species. *Nat. Protoc.* **2013**, *8* (1), 43–51. https://doi.org/10.1038/nprot.2012.142.

(70) Stalhberger, T.; Simenel, C.; Clavaud, C.; Eijsink, V. G. H.; Jourdain, R.; Delepierre, M.; Latgé, J.-P.; Breton, L.; Fontaine, T. Chemical Organization of the Cell Wall Polysaccharide Core of *Malassezia restricta*. *J. Biol. Chem.* **2014**, *289* (18), 12647–12656. https://doi.org/10.1074/jbc.M113.547034.

(71) Ivashov, V. A.; Grillitsch, K.; Koefeler, H.; Leitner, E.; Baeumlisberger, D.; Karas, M.; Daum, G. Lipidome and Proteome of Lipid Droplets from the Methylotrophic Yeast *Pichia pastoris*. *BBA - Mol. Cell Biol. Lipids* **2013**, *1831* (2), 282–290. https://doi.org/10.1016/j.bbalip.2012.09.017.

(72) Petrokilidou, C.; Pavlou, E.; Gaitanis, G.; Bassukas, I. D.; Saridomichelakis, M. N.; Velegraki, A.; Kourkoumelis, N. The Lipid Profile of Three *Malassezia* species Assessed by Raman Spectroscopy and Discriminant Analysis. *Mol. Cell. Probes* **2019**, *46*, 101416. https://doi.org/10.1016/j.mcp.2019.06.006.

(73) Rodrigues, M. L.; Nimrichter, L.; Oliveira, D. L.; Nosanchuk, J. D.; Casadevall, A. Vesicular Trans-Cell Wall Transport in Fungi: A Mechanism for the Delivery of Virulence-Associated Macromolecules? *Lipid Insights* **2008**, *2*, LPI.S1000. https://doi.org/10.4137/LPI.S1000.

(74) Rodrigues, M. L.; Nimrichter, L.; Oliveira, D. L.; Frases, S.; Miranda, K.; Zaragoza, O.; Alvarez, M.; Nakouzi, A.; Feldmesser, M.; Casadevall, A. Vesicular Polysaccharide Export in *Cryptococcus neoformans* Is a Eukaryotic Solution to the Problem of Fungal Trans-Cell Wall Transport. *Eukaryot. Cell* **2007**, *6* (1), 48–59. https://doi.org/10.1128/EC.00318-06.

(75) Rodrigues, M. L.; Nakayasu, E. S.; Oliveira, D. L.; Nimrichter, L.; Nosanchuk, J. D.; Almeida, I.

C.; Casadevall, A. Extracellular Vesicles Produced by *Cryptococcus neoformans* Contain Protein Components Associated with Virulence. *Eukaryot. Cell* **2008**, *7* (1), 58–67. https://doi.org/10.1128/EC.00370-07.

(76) Albuquerque, P. C.; Nakayasu, E. S.; Rodrigues, M. L.; Frases, S.; Casadevall, A.; Zancope-Oliveira, R. M.; Almeida, I. C.; Nosanchuk, J. D. Vesicular Transport in *Histoplasma capsulatum* : An Effective Mechanism for Trans-Cell Wall Transfer of Proteins and Lipids in Ascomycetes. *Cell. Microbiol.* **2008**, *10* (8), 1695–1710. https://doi.org/10.1111/j.1462-5822.2008.01160.x.

(77) Oliveira, D. L.; Nakayasu, E. S.; Joffe, L. S.; Guimarães, A. J.; Sobreira, T. J. P.; Nosanchuk, J. D.; Cordero, R. J. B.; Frases, S.; Casadevall, A.; Almeida, I. C.; Nimrichter, L.; Rodrigues, M. L. Characterization of Yeast Extracellular Vesicles: Evidence for the Participation of Different Pathways of Cellular Traffic in Vesicle Biogenesis. *PLoS One* **2010**, *5* (6), e11113. https://doi.org/10.1371/journal.pone.0011113.

(78) Singh, A.; Del Poeta, M. Lipid Signalling in Pathogenic Fungi. *Cell. Microbiol.* **2011**, *13* (2), 177–185. https://doi.org/10.1111/j.1462-5822.2010.01550.x.

(79) Rella, A.; Farnoud, A. M.; Del Poeta, M. Plasma Membrane Lipids and Their Role in Fungal Virulence. *Prog. Lipid Res.* **2016**, *61*, 63–72. https://doi.org/10.1016/j.plipres.2015.11.003.

(80) Mor, V.; Rella, A.; Farnoud, A. M.; Singh, A.; Munshi, M.; Bryan, A.; Naseem, S.; Konopka, J. B.; Ojima, I.; Bullesbach, E.; Ashbaugh, A.; Linke, M. J.; Cushion, M.; Collins, M.; Ananthula, H. K.; Sallans, L.; Desai, P. B.; Wiederhold, N. P.; Fothergill, A. W.; Kirkpatrick, W. R.; Patterson, T.; Wong, L. H.; Sinha, S.; Giaever, G.; Nislow, C.; Flaherty, P.; Pan, X.; Cesar, G. V.; de Melo Tavares, P.; Frases, S.; Miranda, K.; Rodrigues, M. L.; Luberto, C.; Nimrichter, L.; Del Poeta, M. Identification of a New Class of Antifungals Targeting the Synthesis of Fungal Sphingolipids. *MBio* **2015**, *6* (3). https://doi.org/10.1128/mBio.00647-15.

(81) Lee, J.-H.; Lee, J. Y.; Park, J. H.; Jung, H. S.; Kim, J. S.; Kang, S. S.; Kim, Y. S.; Han, Y. Immunoregulatory Activity by Daucosterol, a β-Sitosterol Glycoside, Induces Protective Th1 Immune Response against Disseminated Candidiasis in Mice. *Vaccine* **2007**, *25* (19), 3834–3840. https://doi.org/10.1016/j.vaccine.2007.01.108.

(82) DeAngelis, Y. M.; Gemmer, C. M.; Kaczvinsky, J. R.; Kenneally, D. C.; Schwartz, J. R.; Dawson,

T. L. Three Etiologic Facets of Dandruff and Seborrheic Dermatitis: *Malassezia* Fungi, Sebaceous Lipids, and Individual Sensitivity. *J. Investig. Dermatology Symp. Proc.* **2005**, *10* (3), 295–297. https://doi.org/10.1111/j.1087-0024.2005.10119.x.

(83) Pandey, A.; Mishra, R. K.; Tiwari, A. K.; Kumar, A.; Bajaj, A. K.; Dikshit, A. Management of Cosmetic Embarrassment Caused by *Malassezia* spp. with Fruticose Lichen Cladia Using Phylogenetic Approach. *Biomed Res. Int.* **2013**, *2013*, 1–8. https://doi.org/10.1155/2013/169794.

(84) Schmidt, C.; Ploier, B.; Koch, B.; Daum, G. Analysis of Yeast Lipid Droplet Proteome and Lipidome. In *Methods in Cell Biology*; 2013; Vol. 116, pp 15–37. https://doi.org/10.1016/B978-0-12-408051-5.00002-4.

(85) Aguilar, L. R.; Pardo, J. P.; Lomelí, M.; Bocardo, O. I. L.; Oropeza Juárez, M.; Sánchez Guerra, G. Lipid Droplets Accumulation and Other Biochemical Changes Induced in the Fungal Pathogen *Ustilago maydis* under Nitrogen - Starvation. *Arch. Microbiol.* **2017**, *199* (8), 1195–1209. https://doi.org/10.1007/s00203-017-1388-8.

(86) Patel, A.; Pruthi, V.; Pruthi, P. A. Innovative Screening Approach for the Identification of Triacylglycerol Accumulating Oleaginous Strains. *Renew. Energy* **2019**, *135*, 936–944. https://doi.org/10.1016/j.renene.2018.12.078.

(87) Adeyo, O.; Horn, P. J.; Lee, S.; Binns, D. D.; Chandrahas, A.; Chapman, K. D.; Goodman, J. M. The Yeast Lipin Orthologue Pah1p Is Important for Biogenesis of Lipid Droplets. *J. Cell Biol.* **2011**, *192* (6), 1043–1055. https://doi.org/10.1083/jcb.201010111.

(88) Bouchez, I.; Pouteaux, M.; Canonge, M.; Genet, M.; Chardot, T.; Guillot, A.; Froissard, M. Regulation of Lipid Droplet Dynamics in *Saccharomyces cerevisiae* Depends on the Rab7-like Ypt7p, HOPS Complex and V1-ATPase. *Biol. Open* **2015**, *4* (7), 764–775. https://doi.org/10.1242/bio.20148615.

(89) Zhang, T.; Chen, S.; Syed, I.; Ståhlman, M.; Kolar, M. J.; Homan, E. A.; Chu, Q.; Smith, U.; Borén, J.; Kahn, B. B.; Saghatelian, A. A LC-MS–Based Workflow for Measurement of Branched Fatty Acid Esters of Hydroxy Fatty Acids. *Nat. Protoc.* **2016**, *11* (4), 747–763. https://doi.org/10.1038/nprot.2016.040.

(90) Zhu, Q.-F.; Yan, J.-W.; Zhang, T.-Y.; Xiao, H.-M.; Feng, Y.-Q. Comprehensive Screening and

Identification of Fatty Acid Esters of Hydroxy Fatty Acids in Plant Tissues by Chemical Isotope Labeling-Assisted Liquid Chromatography–Mass Spectrometry. *Anal. Chem.* **2018**, *90* (16), 10056–10063. https://doi.org/10.1021/acs.analchem.8b02839.

(91) Mannik, J.; Meyers, A.; Dalhaimer, P. Isolation of Cellular Lipid Droplets : Two Purification Techniques Starting from Yeast Cells and Human Placentas. *J. Vis. Exp.* **2014**, *86* (April), 1–10. https://doi.org/10.3791/50981.

(92) Brasaemle, D.; Wolins, N. Isolation of Lipid Droplets from Cells by Density Gradient Centrifugation. *Curr Protoc Cell Biol* **2016**, *72* (1), 3.15.1-3.15.13. https://doi.org/10.1002/cpcb.10.

(93) Sivan, A.; Chet, I. Degradation of Fungal Cell Walls by Lytic Enzymes of *Trichoderma harzianum*. *Microbiology* **1989**, *135* (3), 675–682. https://doi.org/10.1099/00221287-135-3-675.

(94) Ashbee, H. R.; Evans, E. G. V. Immunology of Diseases Associated with *Malassezia Species*. *Clin. Microbiol. Rev.* **2002**, *15* (1), 21–57. https://doi.org/10.1128/CMR.15.1.21-57.2002.

(95) James, G. T. Inactivation of the Protease Inhibitor Phenylmethylsulfonyl Fluoride in Buffers. *Anal. Biochem.* **1978**, *86* (2), 574–579. https://doi.org/10.1016/0003-2697(78)90784-4.

(96) Sharma, A.; Radha Kishan, K. V. Serine Protease Inhibitor Mediated Peptide Bond Re-Synthesis in Diverse Protein Molecules. *FEBS Lett.* **2011**, *585* (21), 3465–3470. https://doi.org/10.1016/j.febslet.2011.10.004.

(97) Wang, X.; Wei, H.; Mao, X.; Liu, J. Proteomics Analysis of Lipid Droplets from the Oleaginous Alga *Chromochloris zofingiensis* Reveals Novel Proteins for Lipid Metabolism. *Genomics. Proteomics Bioinformatics* **2019**, *17* (3), 260–272. https://doi.org/10.1016/j.gpb.2019.01.003.

(98) Ram, A. F. J.; Klis, F. M. Identification of Fungal Cell Wall Mutants Using Susceptibility Assays Based on Calcofluor White and Congo Red. *Nat. Protoc.* **2006**, *1* (5), 2253–2256. https://doi.org/10.1038/nprot.2006.397.

(99) Anthonia O'Donovan, Manimaran Ayyachamy, K. M. T. *Laboratory Protocols in Fungal Biology*; Gupta, V. K., Tuohy, M. G., Ayyachamy, M., Turner, K. M., O'Donovan, A., Eds.; Springer New York: New York, NY, 2013. https://doi.org/10.1007/978-1-4614-2356-0.

(100) R. Malcolm Brown. *Cellulose and Other Natural Polymer Systems*; Brown, R. M., Ed.; Springer US: Boston, MA, 1982. https://doi.org/10.1007/978-1-4684-1116-4.

(101) Wood, P. J. Specificity in the Interaction of Direct Dyes with Polysaccharides. *Carbohydr. Res.* **1980**, *85* (2), 271–287. https://doi.org/10.1016/S0008-6215(00)84676-5.

(102) Knox, J. P. In Situ Detection of Cellulose with Carbohydrate-Binding Modules; 2012; pp 233–245. https://doi.org/10.1016/B978-0-12-415931-0.00012-4.

(103) Greenspan, P.; Mayer, E. P.; Fowler, S. D. Nile Red: A Selective Fluorescent Stain for Intracellular Lipid Droplets. *J. Cell Biol.* **1985**, *100* (3), 965–973. https://doi.org/10.1083/jcb.100.3.965.

(104) Escorcia, W.; Ruter, D. L.; Nhan, J.; Curran, S. P. Quantification of Lipid Abundance and Evaluation of Lipid Distribution in *Caenorhabditis elegans* by Nile Red and Oil Red O Staining. *J. Vis. Exp.* **2018**, No. 133. https://doi.org/10.3791/57352.

(105) Wältermann, M.; Hinz, A.; Robenek, H.; Troyer, D.; Reichelt, R.; Malkus, U.; Galla, H.-J.; Kalscheuer, R.; Stöveken, T.; Von Landenberg, P.; Steinbüchel, A. Mechanism of Lipid-Body Formation in Prokaryotes: How Bacteria Fatten Up. *Mol. Microbiol.* **2004**, *55* (3), 750–763. https://doi.org/10.1111/j.1365-2958.2004.04441.x.

(106) Zuehlsdorff, T. J.; Haynes, P. D.; Payne, M. C.; Hine, N. D. M. Predicting Solvatochromic Shifts and Colours of a Solvated Organic Dye: The Example of Nile Red. *J. Chem. Phys.* **2017**, *146* (12), 124504. https://doi.org/10.1063/1.4979196.

(107) Rumin, J.; Bonnefond, H.; Saint-Jean, B.; Rouxel, C.; Sciandra, A.; Bernard, O.; Cadoret, J.-P.; Bougaran, G. The Use of Fluorescent Nile Red and BODIPY for Lipid Measurement in Microalgae. *Biotechnol. Biofuels* **2015**, *8* (1), 42. https://doi.org/10.1186/s13068-015-0220-4.

(108) Iain Johnson, M. T. Z. S. Probes for Lipids and Membranes. In *Invitrogen™ Molecular Probes™ Handbook: A Guide to Fluorescent Probes and Labeling Technologies*; Life Technologies, 2010.

(109) Daemen, S.; van Zandvoort, M. A. M. J.; Parekh, S. H.; Hesselink, M. K. C. Microscopy Tools for the Investigation of Intracellular Lipid Storage and Dynamics. *Mol. Metab.* **2016**, *5* (3), 153–163. https://doi.org/10.1016/j.molmet.2015.12.005.

(110) Spandl, J.; White, D. J.; Peychl, J.; Thiele, C. Live Cell Multicolor Imaging of Lipid Droplets with a New Dye, LD540. *Traffic* **2009**, *10* (11), 1579–1584. https://doi.org/10.1111/j.1600-0854.2009.00980.x.

(111) Ashbee, H. R.; Evans, E. G. V. Immunology of Diseases Associated with *Malassezia* species. *Clin. Microbiol. Rev.* **2002**, *15* (1), 21–57. https://doi.org/10.1128/CMR.15.1.21-57.2002.

(112) Harris, L.-A. L. S.; Skinner, J. R.; Wolins, N. E. Imaging of Neutral Lipids and Neutral Lipid Associated Proteins; 2013; pp 213–226. https://doi.org/10.1016/B978-0-12-408051-5.00011-5.

(113) Simmons, R. B. Comparison of Chitin Localization in *Saccharomyces cerevisiae*, *Cryptococcus neoformans*, and *Malassezia* spp. *Mycol. Res.* **1989**, *93* (4), 551–553. https://doi.org/10.1016/S0953-7562(89)80053-X.

(114) Wolinski, H.; Kohlwein, S. D. Microscopic Analysis of Lipid Droplet Metabolism and Dynamics in Yeast; Vancura, A., Ed.; Methods in Molecular Biology; Humana Press: Totowa, NJ, 2008; Vol. 457, pp 151–163. https://doi.org/10.1007/978-1-59745-261-8_11.

(115) Yang, H.-J.; Hsu, C.-L.; Yang, J.-Y.; Yang, W. Y. Monodansylpentane as a Blue-Fluorescent Lipid-Droplet Marker for Multi-Color Live-Cell Imaging. *PLoS One* **2012**, *7* (3), e32693. https://doi.org/10.1371/journal.pone.0032693.

(116) Collot, M.; Fam, T. K.; Ashokkumar, P.; Faklaris, O.; Galli, T.; Danglot, L.; Klymchenko, A. S. Ultrabright and Fluorogenic Probes for Multicolor Imaging and Tracking of Lipid Droplets in Cells and Tissues. *J. Am. Chem. Soc.* **2018**, *140* (16), 5401–5411. https://doi.org/10.1021/jacs.7b12817.

(117) Yang, L.; Simionescu, R.; Lough, A.; Yan, H. Some Observations Relating to the Stability of the BODIPY Fluorophore under Acidic and Basic Conditions. *Dye. Pigment.* **2011**, *91* (2), 264–267. https://doi.org/10.1016/j.dyepig.2011.03.027.

(118) Camus, G.; Vogt, D. A.; Kondratowicz, A. S.; Ott, M. Lipid Droplets and Viral Infections. In *Lipid Droplets*; 2013; pp 167–190. https://doi.org/10.1016/B978-0-12-408051-5.00009-7.

(119) Ranall, M.; Gabrielli, B.; Gonda, T. High-Content Imaging of Neutral Lipid Droplets with 1,6-Diphenylhexatriene. *Biotechniques* **2011**, *51* (1). https://doi.org/10.2144/000113702.

(120) Wang, C.-W.; Miao, Y.-H.; Chang, Y.-S. A Sterol-Enriched Vacuolar Microdomain Mediates Stationary Phase Lipophagy in Budding Yeast. *J. Cell Biol.* **2014**, *206* (3), 357–366. https://doi.org/10.1083/jcb.201404115.

(121) Oelkers, P.; Tinkelenberg, A.; Erdeniz, N.; Cromley, D.; Billheimer, J. T.; Sturley, S. L. A Lecithin Cholesterol Acyltransferase-like Gene Mediates Diacylglycerol Esterification in Yeast. *J. Biol. Chem.* **2000**, *275* (21), 15609–15612. https://doi.org/10.1074/jbc.C000144200.

(122) Fujimoto, T.; Parton, R. G. Not Just Fat: The Structure and Function of the Lipid Droplet. *Cold Spring Harb. Perspect. Biol.* **2011**, *3* (3), a004838–a004838. https://doi.org/10.1101/cshperspect.a004838.

(123) Athenstaedt, K. Nonpolar Lipids in Yeast: Synthesis, Storage, and Degradation. In *Biogenesis of Fatty Acids, Lipids and Membranes*; Springer International Publishing: Cham, 2016; pp 1–11. https://doi.org/10.1007/978-3-319-43676-0_22-1.

(124) Athenstaedt, K.; Jolivet, P.; Boulard, C.; Zivy, M.; Negroni, L.; Nicaud, J.-M.; Chardot, T. Lipid Particle Composition of the Yeast *Yarrowia lipolytica* Depends on the Carbon Source. *Proteomics* **2006**, *6* (5), 1450–1459. https://doi.org/10.1002/pmic.200500339.

(125) Fakas, S.; Qiu, Y.; Dixon, J. L.; Han, G.-S.; Ruggles, K. V.; Garbarino, J.; Sturley, S. L.; Carman, G. M. Phosphatidate Phosphatase Activity Plays Key Role in Protection against Fatty Acid-Induced Toxicity in Yeast. *J. Biol. Chem.* **2011**, *286* (33), 29074–29085. https://doi.org/10.1074/jbc.M111.258798.

(126) Kohlwein, S. D. Triacylglycerol Homeostasis: Insights from Yeast. *J. Biol. Chem.* **2010**, *285* (21), 15663–15667. https://doi.org/10.1074/jbc.R110.118356.

(127) Smedes, F.; Thomasen, T. K. Evaluation of the Bligh & Dyer Lipid Determination Method. *Mar. Pollut. Bull.* **1996**, *32* (8–9), 681–688. https://doi.org/10.1016/0025-326X(96)00079-3.

(128) Eggers, L. F.; Schwudke, D. Liquid Extraction: Folch. In *Encyclopedia of Lipidomics*; Springer Netherlands: Dordrecht, 2016; pp 1–6. https://doi.org/10.1007/978-94-007-7864-1_89-1.

(129) Zhang, X.; Yan, S.; Tyagi, R. D.; Drogui, P.; Surampalli, R. Y. Ultrasonication Assisted Lipid Extraction from Oleaginous Microorganisms. *Bioresour. Technol.* **2014**, *158*, 253–261. https://doi.org/10.1016/j.biortech.2014.01.132.

(130) Wrenn, S. P.; Dicker, S. M.; Small, E. F.; Dan, N. R.; Mleczko, M.; Schmitz, G.; Lewin, P. A. Bursting Bubbles and Bilayers. *Theranostics* **2012**, *2* (12), 1140–1159. https://doi.org/10.7150/thno.4305.

(131) Phenomenex INC. High Quality SPE Products https://www.phenomenex.com/Products/Part/8B-S008-FBJ.

(132) Klose, C.; Surma, M. A.; Gerl, M. J.; Meyenhofer, F.; Shevchenko, A.; Simons, K. Flexibility of a Eukaryotic Lipidome – Insights from Yeast Lipidomics. *PLoS One* **2012**, *7* (4), e35063. https://doi.org/10.1371/journal.pone.0035063.

(133) Ivanova, P. T.; Cerda, B. A.; Horn, D. M.; Cohen, J. S.; McLafferty, F. W.; Brown, H. A. Electrospray Ionization Mass Spectrometry Analysis of Changes in Phospholipids in RBL-2H3 Mastocytoma Cells during Degranulation. *Proc. Natl. Acad. Sci.* **2001**, *98* (13), 7152–7157. https://doi.org/10.1073/pnas.131195098.

(134) Han, X.; Gross, R. W. Electrospray Ionization Mass Spectroscopic Analysis of Human Erythrocyte Plasma Membrane Phospholipids. *Proc. Natl. Acad. Sci.* **1994**, *91* (22), 10635–10639. https://doi.org/10.1073/pnas.91.22.10635.

(135) Wang, C.; Wang, M.; Han, X. Applications of Mass Spectrometry for Cellular Lipid Analysis. *Mol. Biosyst.* **2015**, *11* (3), 698–713. https://doi.org/10.1039/C4MB00586D.

(136) Hsu, F.-F.; Turk, J. Characterization of Cardiolipin as the Sodiated Ions by Positive-Ion Electrospray Ionization with Multiple Stage Quadrupole Ion-Trap Mass Spectrometry. *J. Am. Soc. Mass Spectrom.* **2006**, *17* (8), 1146–1157. https://doi.org/10.1016/j.jasms.2006.04.024.

(137) Beckedorf, A. I.; Schäffer, C.; Messner, P.; Peter-Katalinić, J. Mapping and Sequencing of Cardiolipins from *Geobacillus Stearothermophilus* NRS 2004/3a by Positive and Negative Ion NanoESI-QTOF-MS and MS/MS. *J. Mass Spectrom.* **2002**, *37* (10), 1086–1094. https://doi.org/10.1002/jms.369.

(138) Guan, X. L.; Wenk, M. R. Mass Spectrometry-Based Profiling of Phospholipids and Sphingolipids in Extracts from Saccharomyces Cerevisiae. *Yeast* **2006**, *23* (6), 465–477. https://doi.org/10.1002/yea.1362.

(139) Creative Enzymes. Ox bile extract powder https://www.creative-enzymes.com/product/ox-bile-extract-powder_4214.html#:~:text=Bile Extract Powder%2C dried is,characteristics%2C

found in Ox Bile.

(140) Boyer, J. L. Bile Formation and Secretion. In *Comprehensive Physiology*; John Wiley & Sons, Inc.: Hoboken, NJ, USA, 2013. https://doi.org/10.1002/cphy.c120027.

(141) Klompong, V.; Benjakul, S.; Kantachote, D.; Shahidi, F. Characteristics and Use of Yellow Stripe Trevally Hydrolysate as Culture Media. *J. Food Sci.* **2009**, *74* (6), S219–S225. https://doi.org/10.1111/j.1750-3841.2009.01213.x.

(142) Hauton, J. C. Bile Phospholipids : Origin and Function. In *The Hepatobiliary System*; Springer US: Boston, MA, 1976; pp 529–553. https://doi.org/10.1007/978-1-4615-8900-6_25.

(143) Patton, G. M.; Fasulo, J. M.; Robins, S. J. Evidence That Hepatic Triglycerides Provide Acylglycerides for Synthesis of Bile Phosphatidylcholines. *Am. J. Physiol. Liver Physiol.* **1994**, *267* (6), G1028–G1034. https://doi.org/10.1152/ajpgi.1994.267.6.G1028.

(144) Luévano-Martínez, L. A.; Forni, M. F.; dos Santos, V. T.; Souza-Pinto, N. C.; Kowaltowski, A. J. Cardiolipin Is a Key Determinant for MtDNA Stability and Segregation during Mitochondrial Stress. *Biochim. Biophys. Acta - Bioenerg.* **2015**, *1847* (6–7), 587–598. https://doi.org/10.1016/j.bbabio.2015.03.007.

(145) Joshi, A. S.; Zhou, J.; Gohil, V. M.; Chen, S.; Greenberg, M. L. Cellular Functions of Cardiolipin in Yeast. *Biochim. Biophys. Acta - Mol. Cell Res.* **2009**, *1793* (1), 212–218. https://doi.org/10.1016/j.bbamcr.2008.07.024.

(146) Zhou, J.; Zhong, Q.; Li, G.; Greenberg, M. L. Loss of Cardiolipin Leads to Longevity Defects That Are Alleviated by Alterations in Stress Response Signaling. *J. Biol. Chem.* **2009**, *284* (27), 18106–18114. https://doi.org/10.1074/jbc.M109.003236.

(147) Kameoka, S.; Adachi, Y.; Okamoto, K.; Iijima, M.; Sesaki, H. Phosphatidic Acid and Cardiolipin Coordinate Mitochondrial Dynamics. *Trends Cell Biol.* **2018**, *28* (1), 67–76. https://doi.org/10.1016/j.tcb.2017.08.011.

(148) Beltrán-Heredia, E.; Tsai, F.-C.; Salinas-Almaguer, S.; Cao, F. J.; Bassereau, P.; Monroy, F. Membrane Curvature Induces Cardiolipin Sorting. *Commun. Biol.* **2019**, *2* (1), 225. https://doi.org/10.1038/s42003-019-0471-x.

(149) Curtis, J.; Kim, G.; Wehr, N. B.; Levine, R. L. Group B Streptococcal Phospholipid Causes

Pulmonary Hypertension. *Proc. Natl. Acad. Sci.* **2003**, *100* (9), 5087–5090. https://doi.org/10.1073/pnas.0931493100.

(150) Beach, A.; Richard, V. R.; Leonov, A.; Burstein, M. T.; Bourque, S. D.; Koupaki, O.; Juneau, M.; Feldman, R.; Iouk, T.; Titorenko, V. I. Mitochondrial Membrane Lipidome Defines Yeast Longevity. *Aging (Albany. NY).* **2013**, *5* (7), 551–574. https://doi.org/10.18632/aging.100578.

(151) Beach, A.; Richard, V. R.; Bourque, S.; Boukh-Viner, T.; Kyryakov, P.; Gomez-Perez, A.; Arlia-Ciommo, A.; Feldman, R.; Leonov, A.; Piano, A.; Svistkova, V.; Titorenko, V. I. Lithocholic Bile Acid Accumulated in Yeast Mitochondria Orchestrates a Development of an Anti-Aging Cellular Pattern by Causing Age-Related Changes in Cellular Proteome. *Cell Cycle* **2015**, *14* (11), 1643–1656. https://doi.org/10.1080/15384101.2015.1026493.

(152) Marshall, S. E.; Marples, B. A.; Salt, W. G.; Stretton, R. J. Aspects of the Effect of Bile Salts on *Candida Albicans*. *Med. Mycol.* **1987**, *25* (5), 307–318. https://doi.org/10.1080/02681218780000351.

(153) Guinan, J.; Villa, P.; Thangamani, S. Secondary Bile Acids Inhibit *Candida albicans* Growth and Morphogenesis. *Pathog. Dis.* **2018**, *76* (3). https://doi.org/10.1093/femspd/fty038.

(154) Boumann, H. A.; Gubbens, J.; Koorengevel, M. C.; Oh, C.-S.; Martin, C. E.; Heck, A. J. R.; Patton-Vogt, J.; Henry, S. A.; de Kruijff, B.; de Kroon, A. I. P. M. Depletion of Phosphatidylcholine in Yeast Induces Shortening and Increased Saturation of the Lipid Acyl Chains: Evidence for Regulation of Intrinsic Membrane Curvature in a Eukaryote. *Mol. Biol. Cell* **2006**, *17* (2), 1006–1017. https://doi.org/10.1091/mbc.e05-04-0344.

(155) Wang, C.-W.; Miao, Y.-H.; Chang, Y.-S. Control of Lipid Droplet Size in Budding Yeast Requires the Collaboration between Fld1 and Ldb16. *J. Cell Sci.* **2014**, *127* (6), 1214–1228. https://doi.org/10.1242/jcs.137737.

(156) Fruhwirth, G. O.; Loidl, A.; Hermetter, A. Oxidized Phospholipids: From Molecular Properties to Disease. *Biochim. Biophys. Acta - Mol. Basis Dis.* **2007**, *1772* (7), 718–736. https://doi.org/10.1016/j.bbadis.2007.04.009.

(157) Krönke, G.; Leitinger, N. Oxidized Phospholipids at the Interface of Innate and Adaptive Immunity. *Future Lipidol.* **2006**, *1* (5), 623–630. https://doi.org/10.2217/17460875.1.5.623.

(158) Hsu, F.-F.; Turk, J.; Zhang, K.; Beverley, S. M. Characterization of Inositol

Phosphorylceramides from *Leishmania major* by Tandem Mass Spectrometry with Electrospray Ionization. *J. Am. Soc. Mass Spectrom.* **2007**, *18* (9), 1591–1604. https://doi.org/10.1016/j.jasms.2007.05.017.

(159) Heung, L. J.; Luberto, C.; Plowden, A.; Hannun, Y. A.; Del Poeta, M. The Sphingolipid Pathway Regulates Pkc1 through the Formation of Diacylglycerol in *Cryptococcus neoformans*. *J. Biol. Chem.* **2004**, *279* (20), 21144–21153. https://doi.org/10.1074/jbc.M312995200.

XI. Supplementary information

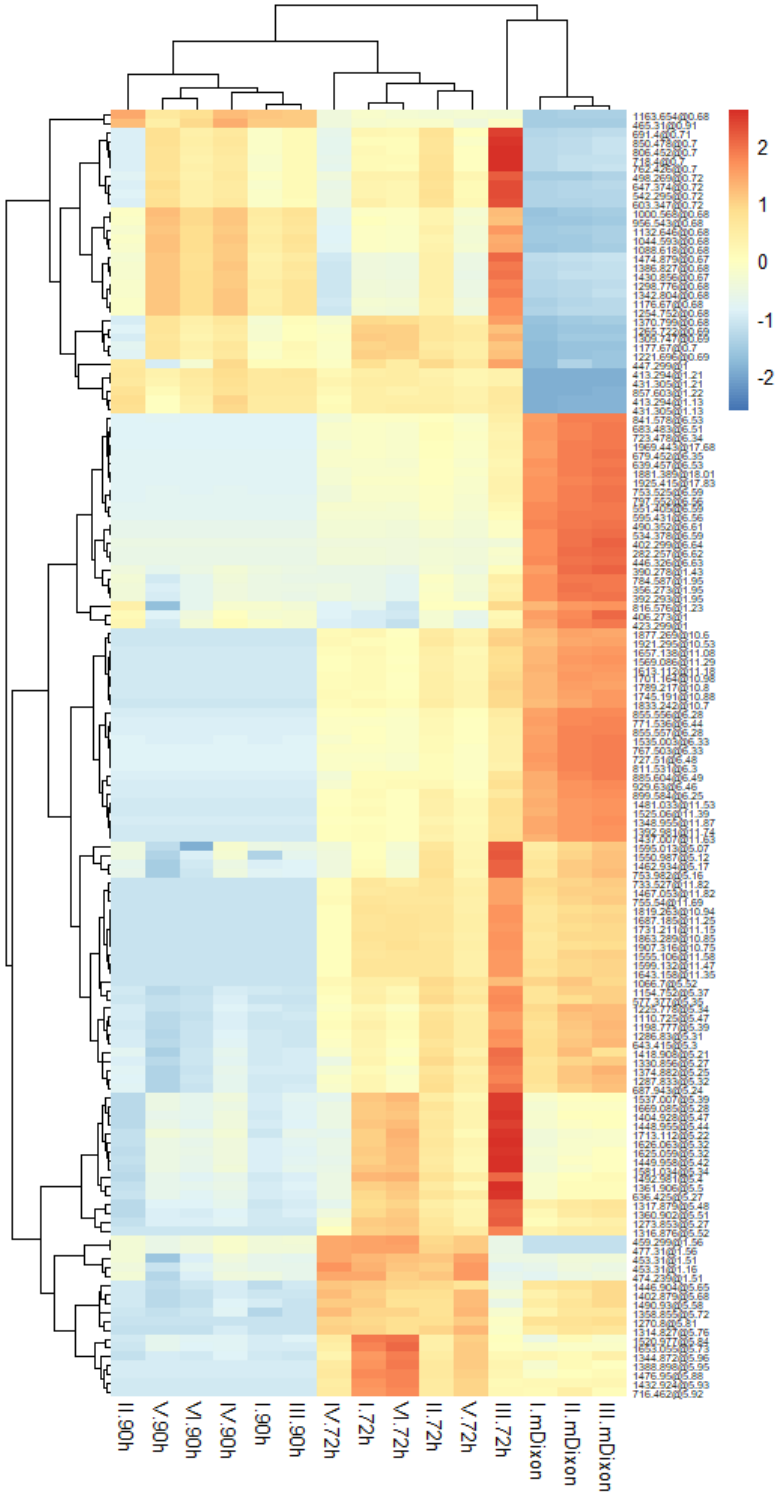

Supplementary figure 1. Heat map of all molecular features identify for differentiation of the fresh mDixon and supernatant of 72h and 90h of *M. globosa* growth. The heatmap denote higher (red) to lower (blue) intensity for each molecular feature.